



Department of mechanical and aeronautical engineering

Course Project: Aerodynamics of a fixed weather drone

MECH-3640 Aerodynamics

By Selim SHERIF
Student ID # 21043926
November 15, 2023

Contents

1 AIRFOIL AERODYNAMICS	1
1.1 Determination of Airfoil Type	1
1.2 Airfoil Characteristics	1
1.2.1 Value of $\alpha_{L=0}$	1
1.2.2 Value of $C_{m,\frac{c}{4}}$	2
1.2.3 Value of x_{cp} and x_{ac}	3
1.3 Lift curves and drag polars	3
1.3.1 Analytical approach	3
1.3.2 Experimental Approach	4
1.3.3 Numerical Approach	6
1.3.4 Comparison and Analysis	6
1.3.5 Pros And Cons of Each Model	8
1.4 Effect of Airfoil Thickness	10
1.4.1 Laminar flow	10
1.4.2 Tripped flow	13
1.4.3 Analysis and Comparisons	15
1.5 Effect of Airfoil Camber	19
1.5.1 Results and Plots	19
1.5.2 Analysis And Comparisons	23
2 WING AERODYNAMICS	24
2.1 Wing Characteristics	24
2.1.1 Static Characteristics	24
2.1.2 Dynamic Characteristics	27
2.2 Numerical model	28
2.3 Effect of Wing Taper Ratio	32
2.4 Effect of Wing Aspect ratio	35
2.4.1 Lift curve and Drag polar	35
2.4.2 Induced drag Analysis	36
2.4.3 VLM VS LLT	38
2.5 Conclusion and final results	39

1 AIRFOIL AERODYNAMICS

1.1 Determination of Airfoil Type

The Airfoil type can easily be deduced visually via the figure shown in the project handout:

- The chord line c is 50 units long and that the airfoil is about 6 units thick at the maximum. Therefore the maximum thickness can be expressed as $\frac{6}{50}c = 0.12c$. By definition the last 2 digits of our 4 digit NACA is given by **12**.
- The maximum distance between the chord line and the camber line is approximately 1 unit, and the distance separating the LE and that point (with respect to the chord line) is approximately 20 units i.e. $\frac{20}{50}c = 0.4c$. The 2nd digit of our NACA number is in that case **4**
- Finally, the first digit of a NACA 4 digit airfoil is given by the maximum camber which in this case represents 2% of c (1 unit). So the first digit of our NACA airfoil is **2**

The Airfoil type is a **NACA 2412**

1.2 Airfoil Characteristics

In the following section, we assume that all TAT conditions are satisfied and that the TAT model can be safely applied.

1.2.1 Value of $\alpha_{L=0}$

We will firstly determine the zero lift angle of attack $\alpha_{L=0}$.

For a general 4-digit NACA airfoil, the equation of the camber line is as follows :

$$z = \begin{cases} \frac{m}{p^2} \left(2px - \frac{x^2}{c} \right) & 0 \leq x \leq pc \\ \frac{m}{(1-p)^2} \left((1-2p)c + 2px - \frac{x^2}{c} \right) & pc \leq x \leq c \end{cases} \quad (1)$$

In this specific case : $m = 0.02$ and $p = 0.4$ Which can be used to re-write (1) as :

$$z = \begin{cases} 0.125 \left(0.8x - \frac{x^2}{c} \right) & 0 \leq x \leq 0.4c \\ \frac{1}{18} \left(0.2c + 0.8x - \frac{x^2}{c} \right) & 0.4c \leq x \leq c \end{cases} \quad (2)$$

Taking the derivative with respect to x , we get the following:

$$\frac{dz}{dx} = \begin{cases} 0.1 - 0.25\frac{x}{c} & 0 \leq x \leq 0.4c \\ \frac{2}{45} - \frac{x}{9c} & 0.4c \leq x \leq c \end{cases} \quad (3)$$

Substituting to enter the polar coordinate system we get

$$x = \frac{c}{2}(1 - \cos\theta)$$

and

$$\frac{dz}{d\theta} = \begin{cases} 0.1 - 0.25\frac{(1-\cos\theta)}{\frac{c}{2}} & 0 \leq x \leq 0.4c \\ \frac{2}{45} - \frac{(1-\cos\theta)}{\frac{18}{c}} & 0.4c \leq x \leq c \end{cases}$$

For the boundary conditions, we can simply take the first one as an example :

$$\begin{aligned}
 0 &\leq x \leq 0.4c \\
 \Leftrightarrow 0 &\leq \frac{1}{2}(1 - \cos \theta) \leq 0.4 \\
 \Leftrightarrow 0 &\leq 1 - \cos \theta \leq 0.8 \\
 \Leftrightarrow -1 &\leq -\cos \theta \leq -0.2 \\
 \Leftrightarrow 1 &\geq \cos \theta \geq 0.2 \\
 \Leftrightarrow 0 &\leq \theta \leq \arccos(0.2)
 \end{aligned}$$

which leads to :

$$\frac{dz}{dx} = \begin{cases} 0.1 - 0.25 \frac{(1 - \cos \theta)}{2} & 0 \leq \theta \leq \arccos(0.2) \\ \frac{2}{45} - \frac{(1 - \cos \theta)}{18} & \arccos(0.2) \leq \theta \leq \pi \end{cases} \quad (4)$$

The zero lift angle of attack $\alpha_{L=0}$ can now be directly determined via the following formula

$$\alpha_{L=0} = -\frac{1}{\pi} \int_0^\pi \frac{dz}{dx} (\cos \theta - 1) d\theta \quad (5)$$

$$\Leftrightarrow \alpha_{L=0} = -\frac{1}{\pi} \left(\int_0^{\arccos(0.2)} \frac{dz}{dx} (\cos \theta - 1) d\theta + \left(\int_{\arccos(0.2)}^\pi \frac{dz}{dx} (\cos \theta - 1) d\theta \right) \right) \quad (6)$$

Inserting equation (4) we get

$$\Leftrightarrow \alpha_{L=0} = -\frac{1}{\pi} \left(\int_0^{\arccos(0.2)} \left(0.1 - 0.25 \frac{(1 - \cos \theta)}{2} \right) (\cos \theta - 1) d\theta + \left(\int_{\arccos(0.2)}^\pi \left(\frac{2}{45} - \frac{(1 - \cos \theta)}{18} \right) (\cos \theta - 1) d\theta \right) \right) \quad (7)$$

Using an online calculator we conclude :

$$\Leftrightarrow \alpha_{L=0} \approx -0.0076611383 - 0.079928382 + 0.0389321305 + 0.012402706 \approx -0.0363 rad \approx -2.0772404^\circ \quad (8)$$

The zero lift angle of attack in this case is approximately -2.08°

1.2.2 Value of $C_{m,\frac{c}{4}}$

Now let's compute the moment coefficient about the quarter chord $C_{m,\frac{c}{4}}$. For this, we need to calculate the respective coefficients A_1 and A_2

By definition :

$$A_1 = \frac{2}{\pi} \int_0^\pi \frac{dz}{dx} \cos(\theta) d\theta \quad A_2 = \frac{2}{\pi} \int_0^\pi \frac{dz}{dx} \cos(2\theta) d\theta \quad (9)$$

We can first compute A_1 using equation (4) :

$$A_1 = \frac{2}{\pi} \left(\int_0^{\arccos(0.2)} \left(0.1 - 0.25 \frac{(1 - \cos \theta)}{2} \right) \cos(\theta) d\theta + \left(\int_{\arccos(0.2)}^\pi \left(\frac{2}{45} - \frac{(1 - \cos \theta)}{18} \right) \cos(\theta) d\theta \right) \right) \quad (10)$$

Which we calculate viz an online calculator:

$$A_1 \approx \frac{2}{\pi}(0.07334245 + 0.05466981) \approx 0.0815$$

Using the same reasoning we can find the value of A_2 :

$$A_2 \approx \frac{2}{\pi}(0.03919184 - 0.01741859) \approx 0.0138$$

Such that:

$$A_1 \approx 0.0815 \quad A_2 \approx 0.0138 \quad (11)$$

We can finally find the value of $C_{m,\frac{c}{4}}$ with the following definition :

$$\begin{aligned} C_{m,\frac{c}{4}} &= \frac{\pi}{4}[A_2 - A_1] \\ \Leftrightarrow C_{m,\frac{c}{4}} &\approx -0.0532 \end{aligned} \quad (12)$$

1.2.3 Value of x_{cp} and x_{ac}

With this information we can now compute the center of pressure x_{cp} . By definition the center of pressure is given by :

$$x_{cp} = \frac{c}{4} \left[1 + \frac{\pi}{C_l} (A_1 - A_2) \right]$$

with

$$C_l = 2\pi(\alpha - \alpha_{L=0})$$

Therefore :

$$x_{cp} = \frac{c}{4} \left[\frac{2(\alpha - \alpha_{L=0}) + (A_1 - A_2)}{2(\alpha - \alpha_{L=0})} \right] \quad (13)$$

Replacing by the corresponding values :

$$x_{cp} = \frac{c}{4} \left[\frac{2\alpha + 0.1403}{2\alpha + 0.726} \right] \quad (14)$$

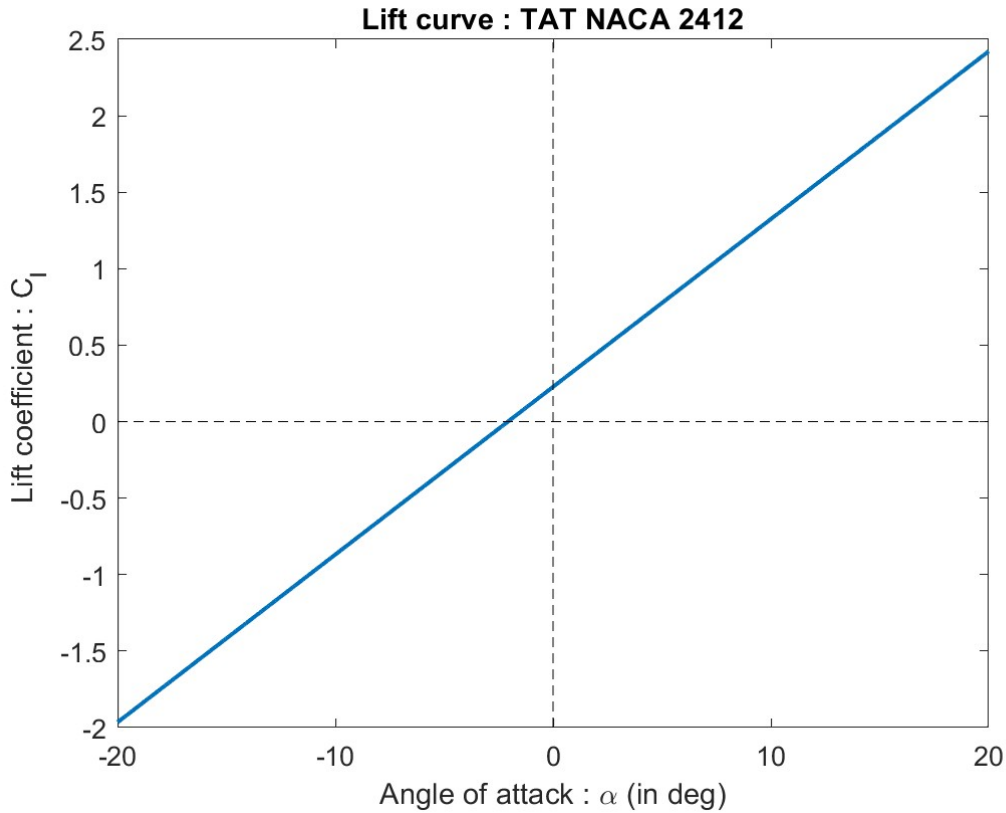
Finally we must note that the aerodynamic center is always at the quarter chord length (NACA Airfoil):

$$x_{ac} = \frac{c}{4} \quad (15)$$

1.3 Lift curves and drag polars

1.3.1 Analytical approach

The lift curve can be deduced analytically via the previous calculations and has the following shape:



The equation for this line is:

$$C_l = 2\pi(\alpha - \alpha_{L=0}) \approx \frac{\pi^2}{90}(\alpha + 2.08) \quad (16)$$

For the drag polar, the TAT model cannot and does not predict the shape of the drag polar (It includes 0 information about the drag).

1.3.2 Experimental Approach

Before we can discuss and interpret any of the important results of the wind tunnel experiments we must firstly estimate the Reynolds number.

The Reynolds's number is defined to be:

$$R_e = \frac{\rho V_\infty c}{\mu}$$

- The following data was measured on the day of the lab :

$$p = 100 \text{ kPa} \quad T = 24.5^\circ \text{C} \quad \text{Humidity} = 72\%$$

- The characteristic length of an airfoil is , according to ChatGPT, the chord length c . The lab sheet states that our chord length c is :

$$c = 100 \text{ mm}$$

- The speed in the wind tunnel was set to :

$$V_\infty = 23 \text{ m/s}$$

- The dynamic viscosity of air is a function of the temperature and can therefore be easily determined:

$$\mu_{T=24.5^\circ\text{C}} = 18.34 * 10^{-6} \text{ Pa.s}$$

- The air density is a function that depends on the temperature, the humidity and the pressure and can be calculated directly online :

$$\rho(T = 24.5^\circ\text{C}, \text{Humidity} = 72\%, p = 100 \text{ kPa}) = 1.1606 \frac{\text{kg}}{\text{m}^3}$$

Therefore the Reynolds number is estimated by :

$$R_e \approx 14.55 * 10^4 \quad (17)$$

This Reynold's number will also be used later for the numerical approach.

At this point we can proceed to plot and interpret the experimental data. During the wind tunnel lab we extracted the lift and drag coefficients forces that the wing induces. With these numbers it is very easy to calculate the respective lift (and drag) coefficients with the following formula's :

$$C_L = \frac{F_L}{\frac{1}{2}\rho V_\infty^2} \quad (18)$$

and

$$C_D = \frac{F_D}{\frac{1}{2}\rho V_\infty^2} \quad (19)$$

We can input our values (The surface is given in the lab handout)

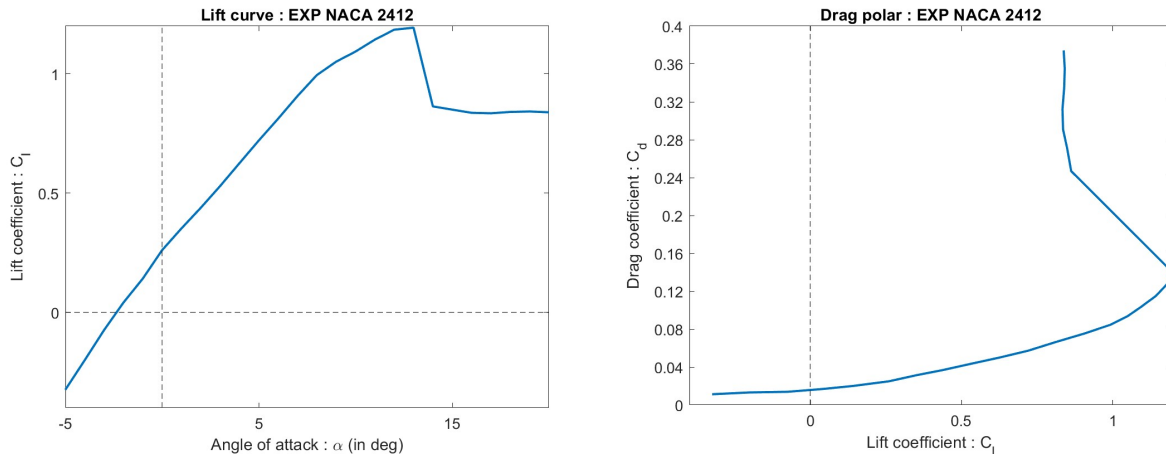
$$\rho = 1.1606 \frac{\text{kg}}{\text{m}^3} \quad V_\infty = 23 \frac{\text{m}}{\text{s}} \quad S = c * L = 0.0395 \text{ m}^2$$

To get the following relations:

$$C_L \approx 0.0825 F_L \quad (20)$$

$$C_D \approx 0.0825 F_D \quad (21)$$

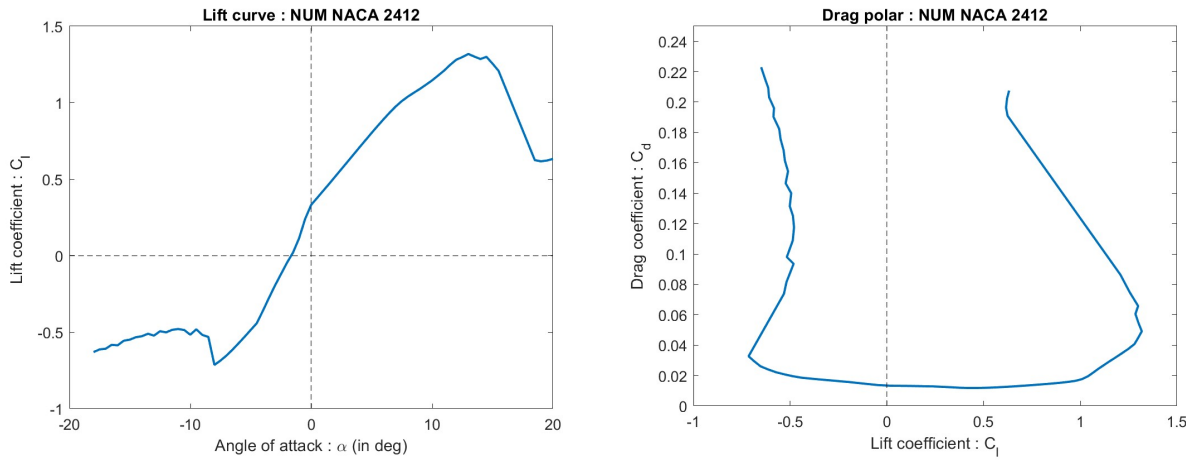
The resulting graphs are as follows :



1.3.3 Numerical Approach

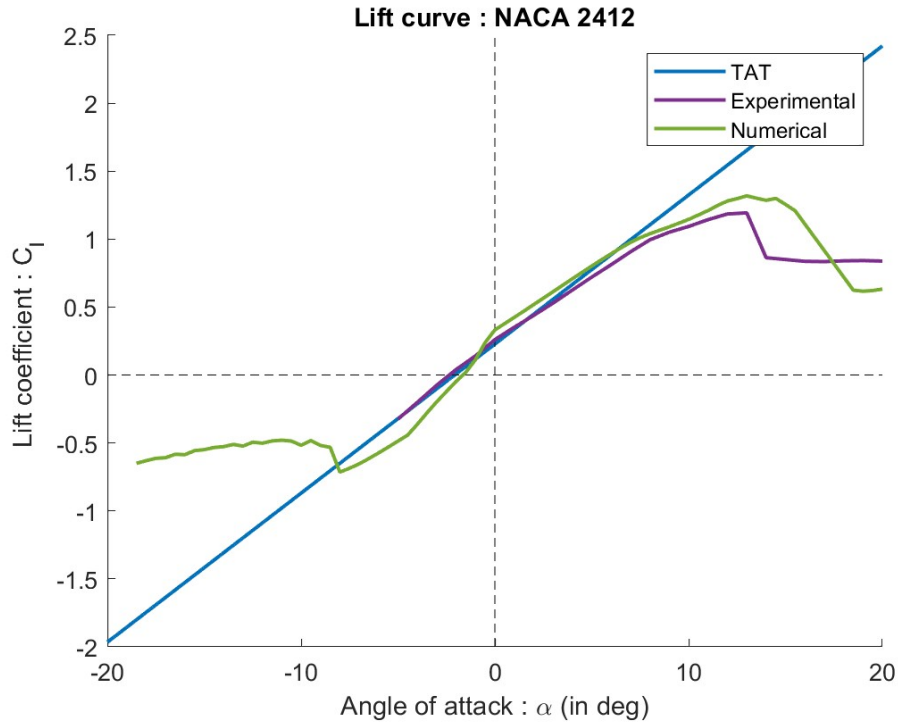
For our simulations we will use the same Reynolds's number as the one measured during the lab tests i.e. $R_e \approx 14.55 * 10^4$.

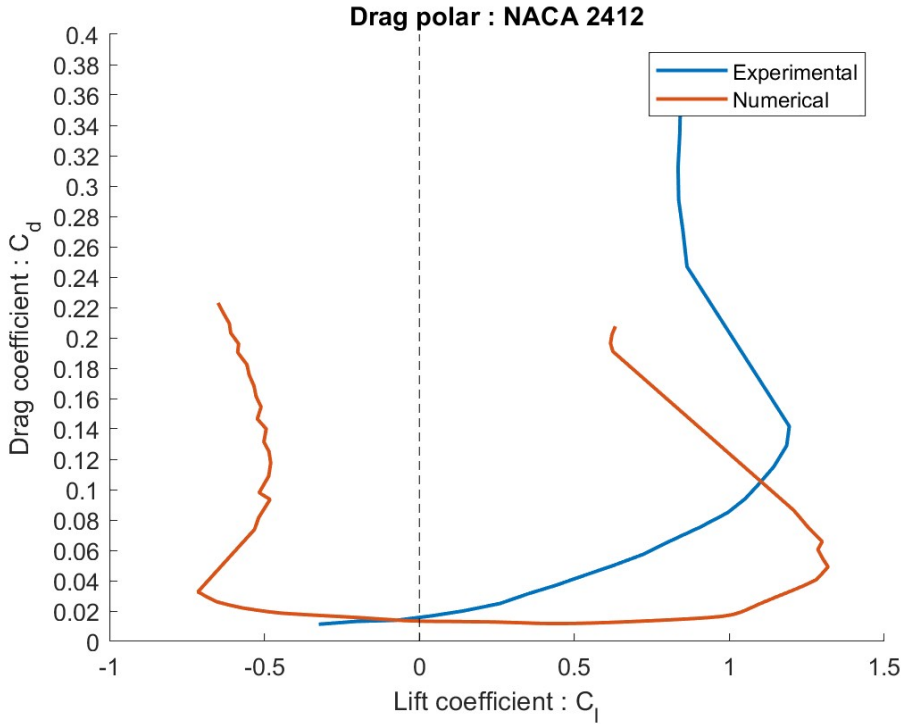
Using XFLR5 for the numerical simulations we get the following results for our NACA 2412:



1.3.4 Comparison and Analysis

Before comparing the different plots and curves, it would be interesting to draw a plot that combines all of the 3 approaches used previously :





Lets start by analyzing the **lift curves** of our NACA 2412 :

- Firstly and foremost, we must note the incredible correlation and similarity in behavior between the 3 models in the intermediate regime (when $\alpha \in [-8; 8]$). The three models predict with near perfection a linear behavior between the angle of attack and the lift coefficient. This result must not be understated even though it might seem obvious at first. The three approaches used are totally unique and are derived from 3 totally different sources: One uses the fundamental laws of physics combined with simplification and assumptions to approach analytically (without doing a single simulation or experiment) the behavior of the airfoil, whilst the second one uses thousands of computer calculations and permutations to find the behavior of the wing. The final approach is just the real-world physical thing with real life parameters (no calculation involved or needed). Yet all 3 drastically different approaches lead to the same trend and the same curve which is remarkable.
- The stall drop can be observed for the experimental and numerical curves, however the TAT model, as expected, does not predict the stall drop. This is obviously due to the fact that many hypotheses and assumptions where imposed when the TAT model was derived (Perfect smooth irrotational non-viscous flow, no flow separation/turbulence, perfect wing...). Therefore in that sense the TAT model can only be used to predict the behavior of the airfoil in the intermediate stage but not when the airfoil is close to the stalling angle of attack where it starts to deviate form the practical results, and to fail as a model.
- The stalling phenomenon appears at respectively and approximately 13° and 15° for the experimental curve and the numerical curve. This can be explained by many factors including the precision of the alignment of the wing during the experiment or the algorithms and systems of equations used to do the numerical simulation as these simulations are more or less precise depending on the algorithm used and on the situation there are used in.

- Furthermore, it must be noted that the stall phenomena happens on a larger range of α for the numerical approach as opposed to the experimental one. This can again be explained by the fact that the algorithm does not necessarily predict the behavior of turbulent flow correctly or precisely as that it is an approximation. For a thickness 12 NACA Wing, the literature suggests that the prominent type of stall is leading edge stall. In this case, the experimental approach is more proximate to that prediction due to the abrupt drop during stall (that can be seen on the experimental curve) which is a characteristic of LE stall.

Now let us Analyze the **Drag Polars**:

- Most important is the fact that TAT fails to predict the shape of the drag polar and does not give us any relationship between the drag coefficient and the lift coefficient. This is due to the simple fact that the TAT model assumes no viscous forces (i.e. no drag)
- In the intermediate part of the graph ($C_d \in [0; 0.6]$), the numerical curve is nearly a horizontal one. In other words, the numerical approach predicts that in this part, an increase in lift coefficient will NOT induce any change in the drag coefficient. This relationship seems counter-intuitive and non-physical (There is no such thing as free lift. In physics everything comes at a price), as intuition would tell us that for an increase in lift, there must be an increase in drag (specially for a range of C_l as big as this one). And indeed, this is what the experimental approach predicts : The experimental drag polar exposes an increasing relationship between C_l and C_d (meaning an increase in the lift induces an increase in drag) which makes a lot of sense intuitively.
- The sharp slope change occurs for both polars at approximately $C_l = 1.3$, However it occurs at $C_d = 0.05$ for the numerical drag polar and $C_d = 0.13$. This again can be interpreted as the fact that the experimental approach predicts a much more correlated and synchronized relationship between the increase in C_l and in C_d . This can again be explained by the flaws and inaccuracies of the algorithm and the models (TAT is in the background of all of this) used by XFLR5

1.3.5 Pros And Cons of Each Model

After these results let's list all the pros and cons of the different models

Analytical Approach

- **Pros**

- Does not need any supplementary material or technological tools : Just pen and paper.
- Relatively straightforward, mechanical and rigorous.
- Easy to apply.
- The result is a very simple linear mathematical model : Easy to manipulate and to implement in other applications.

- **Cons**

- Too many initial approximations and assumptions : Can only be applied in very particular situations and conditions (Laminar, non-viscous, irrotational, no manufacturing imperfections...)
- Fails to predict stall point and to predict the drag polar shape due to assumptions.

- Theoretical : cannot predict real-world uncertainty and unexpected events.
- Long and laborious integrals :)

Experimental Approach

- Pros

- Closest one to predict what will actually happen to the real full scale wing.
- Takes into account and predicts all unexpected and uncalculated phenomena and warns the designer in case one appears.

- Cons

- Needs lots of resources : Wind tunnel facility, wing prop ...
- Not very cost efficient and very energy consuming.
- Needs lots of preparation before the testing, and lots accuracy during the setup.
- High Risk : The wind tunnel tests are usually done only once, so failure to do the test is not a very good idea (lots of time and money lost).

Numerical Approach

- Pros

- Probably the most practical: Good balance between theoretical/analytical knowledge and applied knowledge
- Very time efficient and only utilizes a computer (easy to setup).
- Gives relatively good predictions (relative to TAT) and is widely used in the industry for its efficiency.
- Good ROI in terms of efforts vs precise results.

- Cons

- Can sometimes be misleading and incorrect if the used software or type of simulation is not adequate to the situation.
- Cannot predict certain unexpected natural phenomena and hard to simulate turbulence.
- Still does not 100% predict what the real-world flow will look like (but close enough).

1.4 Effect of Airfoil Thickness

The six airfoils considered are as follows:

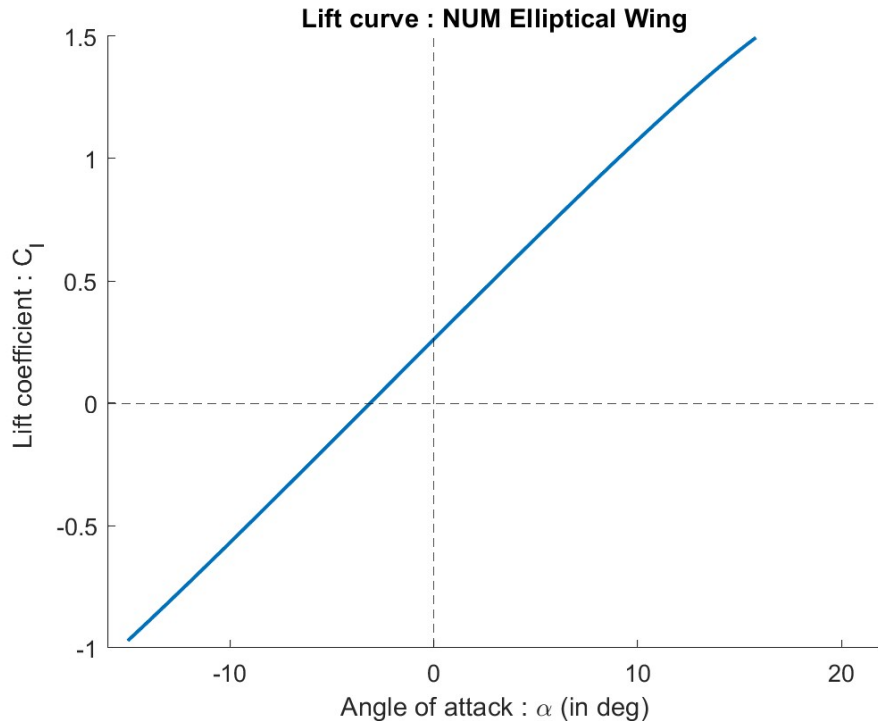
NACA Number	Relative Thickness
2406	-6%
2409	-3%
2412	Reference
2415	3%
2418	6%
2421	9%

We will use these different airfoils to try and understand the effect of wing thickness on the flight dynamics of the airfoil. We will firstly analyze how the airfoil thickness affects the dynamics when it is subjected to a smooth laminar flow, then we will see what happens when the airfoil faces a tripped turbulent flow :

1.4.1 Laminar flow

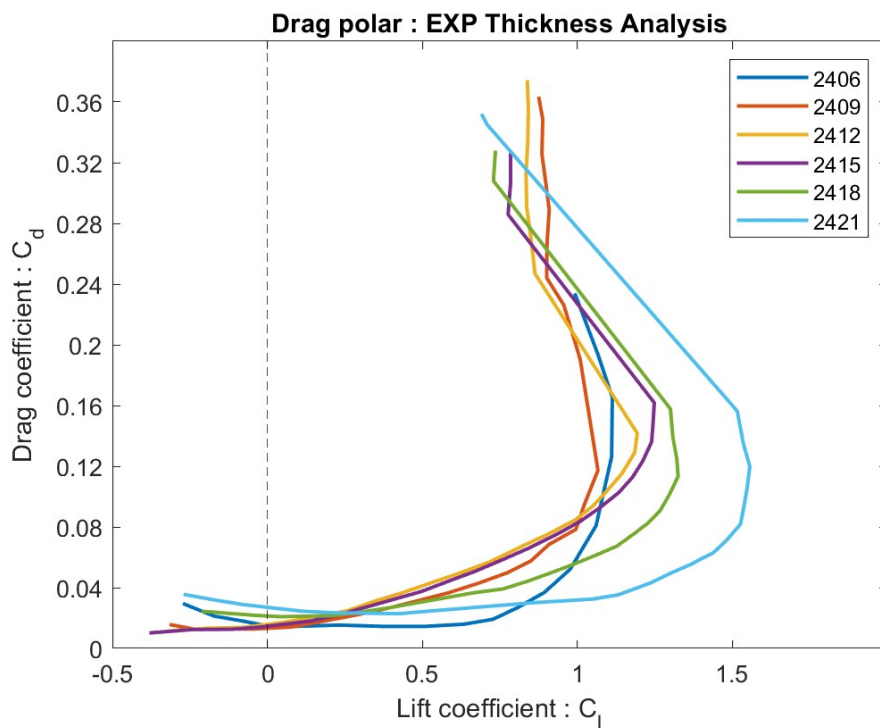
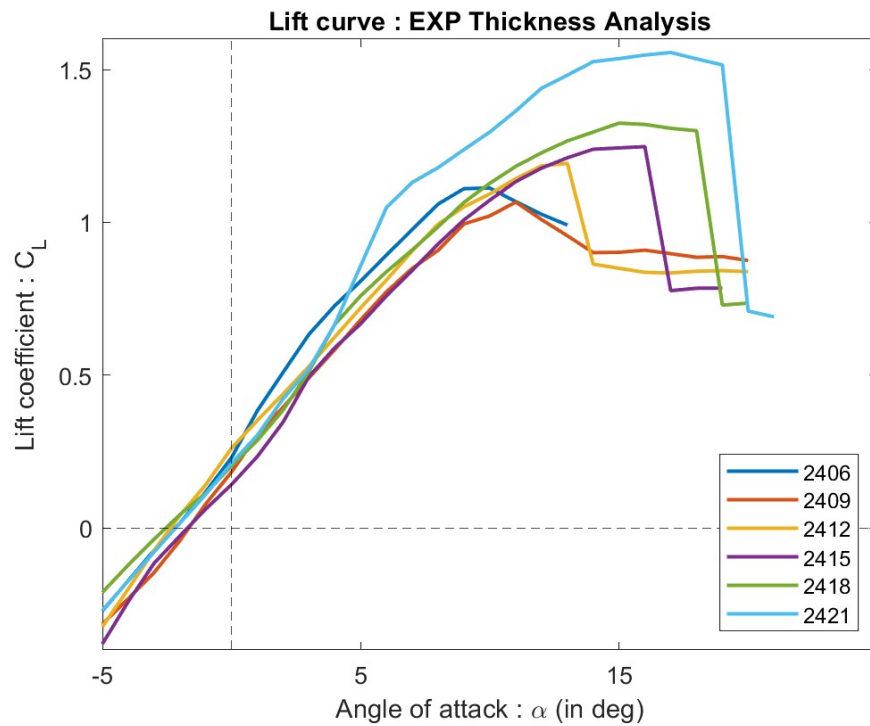
- **Analytical Approach**

Firstly and foremost, like in the previous case, TAT fails to predict the shape of the drag polar diagram. Therefore, in this regard no new information can be extracted. However, for the lift curve TAT predicts that the lift coefficient as a function of α is independent of the airfoil thickness. In other words, **the lift curve is the same for all airfoils considered in this subsection and is the same as the NACA 2412 previously discussed :**



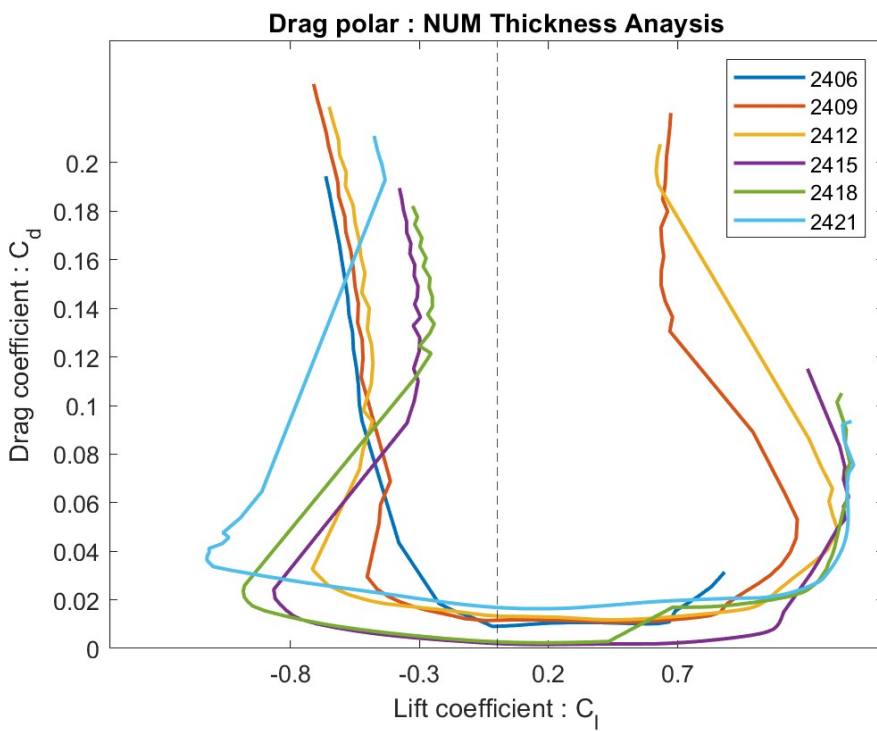
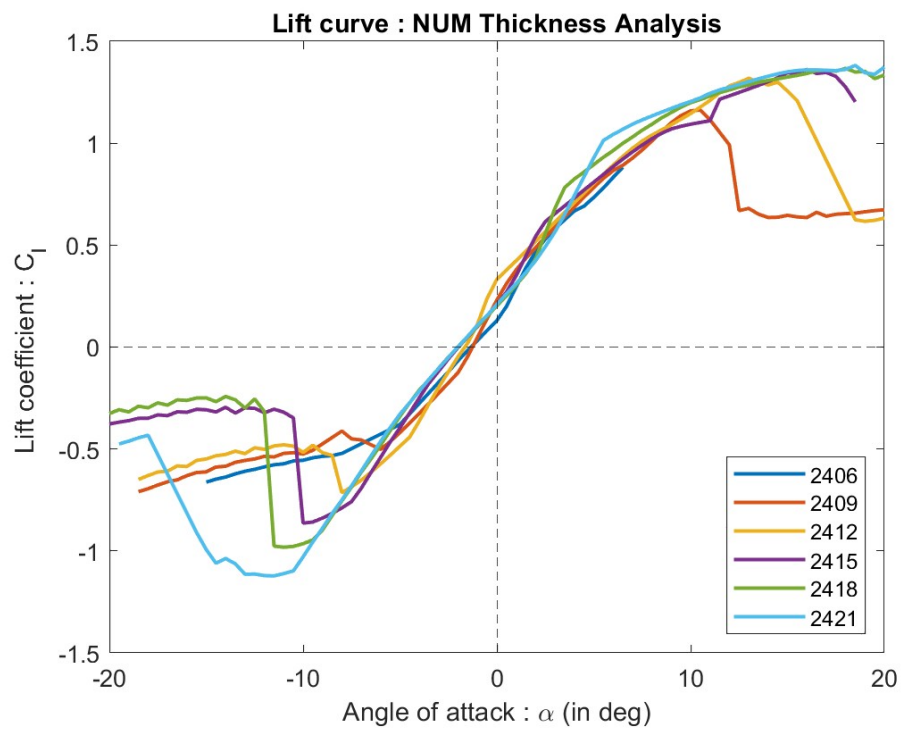
- **Experimental Approach**

Using the same formulas as previously for the lift and drag coefficients, we can plot the following curves :



- Numerical Approach

The Numerical approach for these airfoils yields :

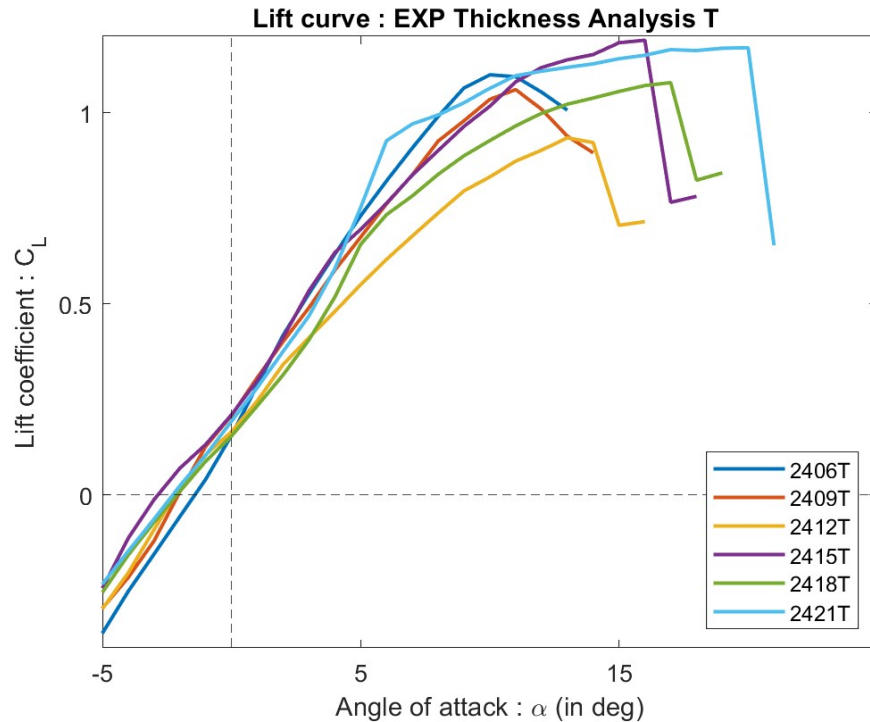


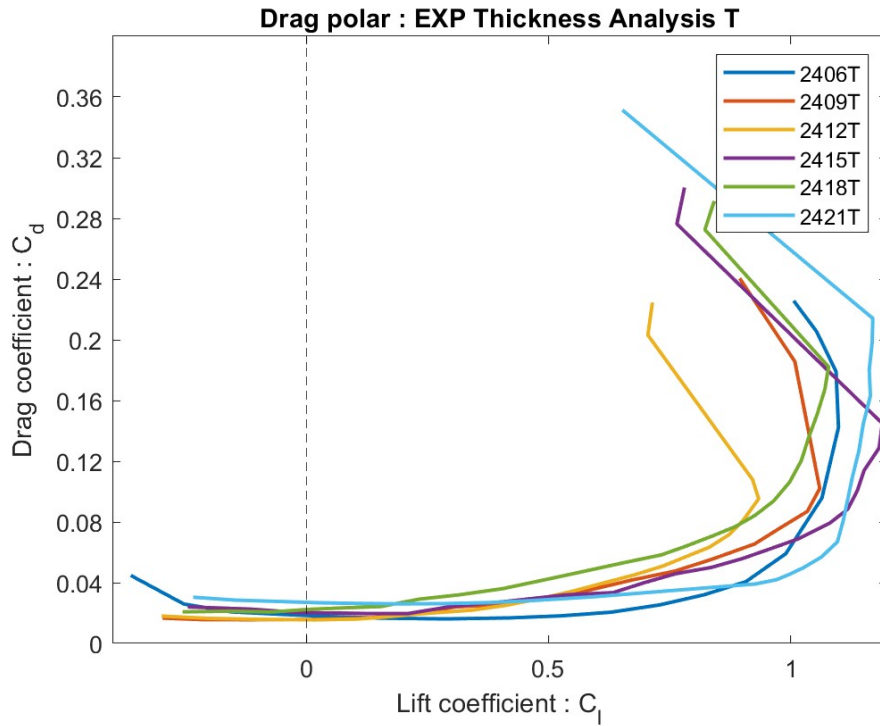
1.4.2 Tripped flow

- **Analytical Approach**

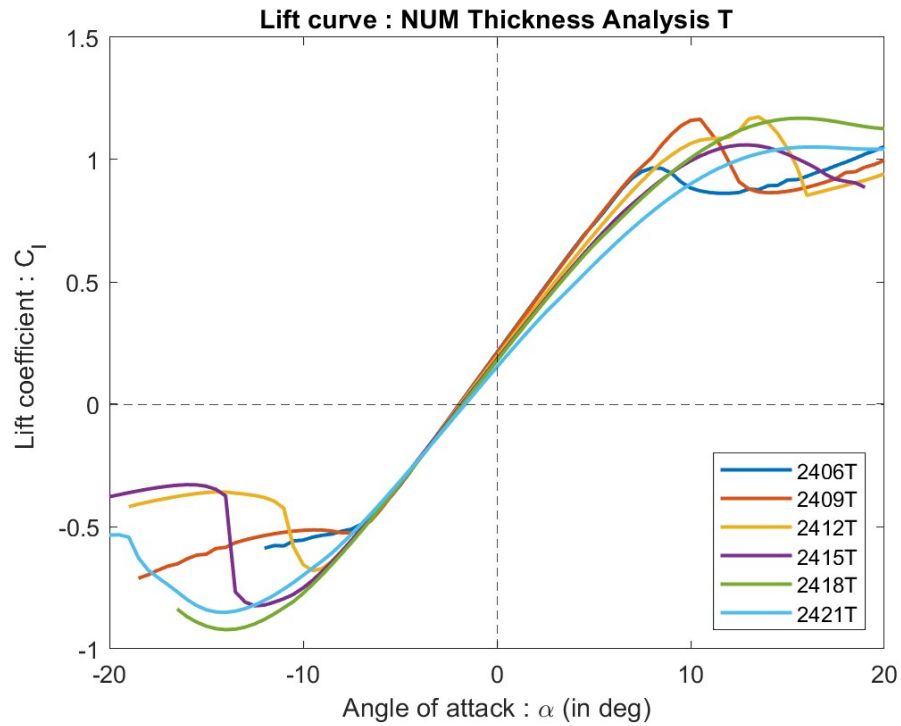
One of the key characteristics and hypotheses of TAT Model is to suppose laminar non-viscous irrotational flow. This means that considering a tripped flow with the TAT model doesn't make sense physically and mathematically but it is also an impossible task to do.

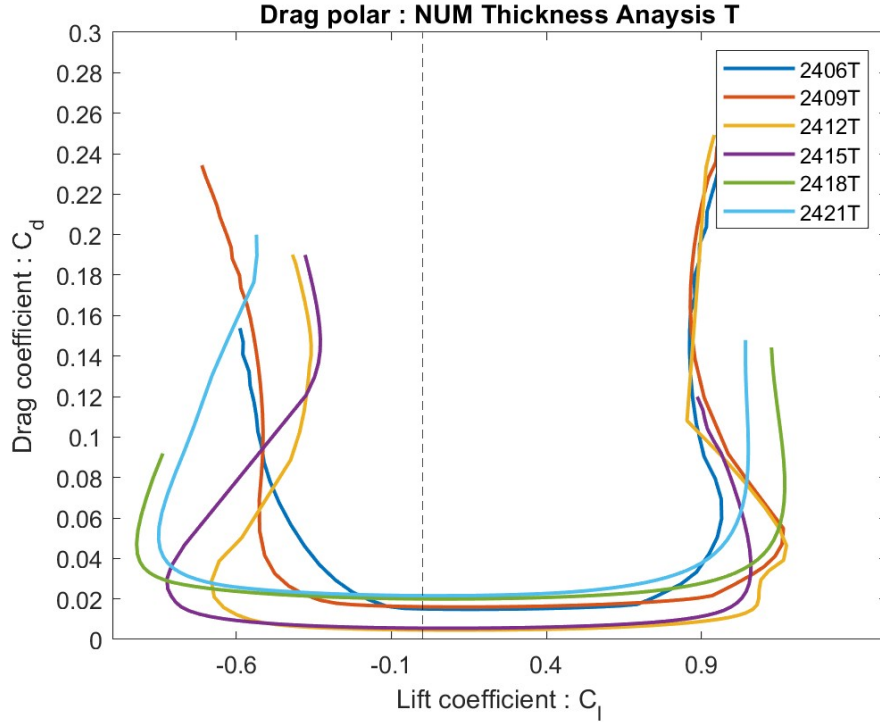
- **Experimental Approach**





- Numerical Approach





1.4.3 Analysis and Comparisons

Firstly, let us deduce the effect of wing thickness on lift and drag using the data of both the tripped flow and the laminar flow as they are both consistent with regard to the influence of thickness :

- As predicted by TAT model, during the intermediate regime when the angle of attack is not close to the stall angle, we realize that the slope of the curve and that x-intercept of the lift curve are totally independent from the airfoil thickness. This is translated physically by the fact that the zero lift angle of attack does not depend on the airfoil thickness.

Data from the laminar flow both numerical and experimental clearly show the superposition of the different curves (which represent different thicknesses).

The tripped flow also shows the same superposition, however this time the correlation is not as pronounced, we see subtle differences and separation. Specifically looking at the numerical tripped thickness lift curve, we realize that the slope varies (a tiny bit) as a function of the thickness (and of the angle of attack obviously). This is justified by the tripped flow being turbulent (and there can be no turbulence without viscosity). Therefore viscous effects directly affect the correlation and play a role in the relationship, as opposed to the clean airflow case or the TAT case where the effect of viscosity can be negligible and not as significant. The effect mentioned seems to be a decrease of the slope of the lift curve.(Note that the thicker airfoils are the ones affected the most by this, probably because they induce more drag (they are bigger) and so this viscous effect is the strongest on them). And that is main reason very thick aifoils are avoided: High drag !

- The stall phenomenon and its relationship to the thickness of the airfoil in this case is very interesting:

- In general, the tendency is that the thicker the wing, the higher the angle of attack is needed to provoke stall. This can consistently be seen for both experimental and

numerical, and, for both tripped and laminar flow, where the stall drop is generally observed later for the thicker airfoils and vice versa for the thinner ones.

- As the literature mentions, we can identify 3 types of stall : TA stall for thin airfoils, LE stall for intermediate size airfoils and TE stall for thick airfoils. Although in this case there is lots of variability and differences between the plots we can **on average** classify the different airfoils as follows:

TA stall: 2406 (dark blue); 2409 (red)

LE stall: 2409 (red); 2412 (yellow); 2415(purple)

TE stall: 2415 (purple); 2418 (green); 2421 (light blue)

As shown, some airfoils appear in 2 categories as they are ambiguous (depending on the graph) and behave as a transition between the different classes.

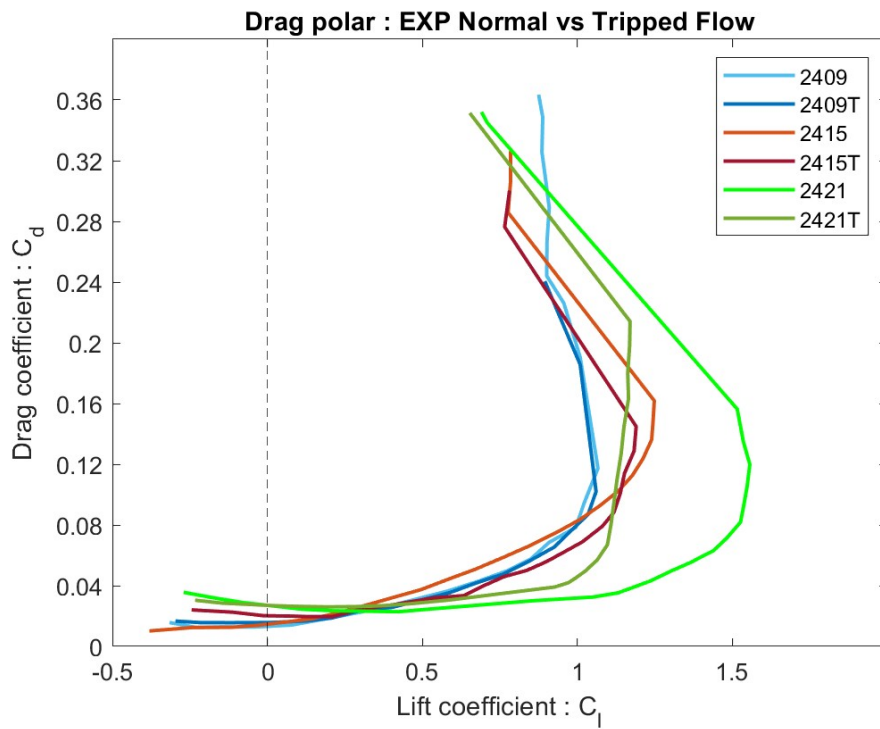
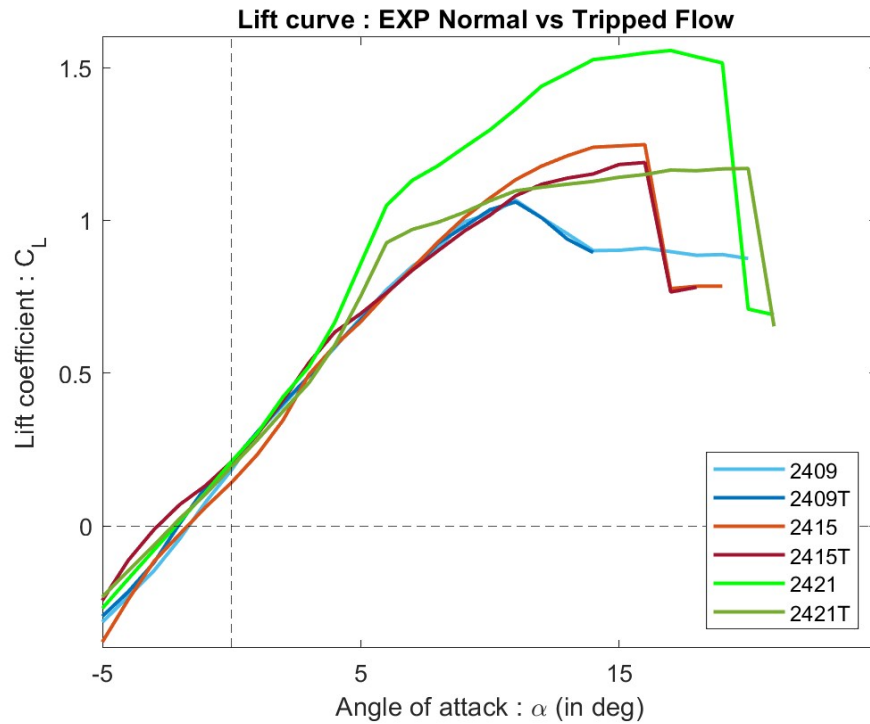
In general, the difference between the different types of stall are more pronounced and distinguishable in the numerical experiments than the experimental ones. This is a result of many factors, one them being that the data from the numerical approach is much more dense and evenly spread than the experimental data which maybe does not describe precisely the real shape of the stall drop (i.e. there is not enough data points to accurately model the shape of the drop. In general the drop is a very interesting area of the curve and needs more data to be accurately represented than the rest of the curve because there is so much information in such a short span of time)

- We must distinguish the difference between LE stall behavior and TE behavior. In general, the LE stall happens at a sharp peak but more abruptly and quickly as opposed the TE stall which happens usually at flush peak that decreases gradually (which is a better behavior for aircraft design). This can be observed in our data sets with the best one showcasing this being the tripped numerical lift curve.
- It is important to note that the highest possible C_l 's are in general not achieved by the thicker airfoils, but by the airfoils who produce LE stall. This is due to the sharp tip/peak mentioned in the previous point that is a characteristic behavior of LE stall.
- For the drag polar, the tendency here is that the base of the drag polar is generally much wider for thicker airfoils. This is true for all the data whether numerical or experimental, tripped or not, and can be translated by the fact that thicker airfoils can have a bigger lift coefficient for a given drag coefficient. The intuitive explanation here is again the fact that stall occurs much later for the thicker wing compared to the thinner ones due to TE stall which leads to a wider range in C_l if we restrict our C_d to a relatively reasonable number.
- There is, as usual, an intermediate range ($C_l \in [-0.3; 0.7]$) where all the different airfoils behave in the exact same matter, meaning that for this interval of C_l airfoil thickness does not matter.
- For the numerical data, the drag polars are approximately all symmetric about same axis ($x \approx 0.2$) meaning that the thickness does not shift the polar graph to the right or to the left. In other words, the interval over which the relationship of the lift and drag behaves in a quasi-linear steady way does not change with regard to the thickness (before the drag coefficient explodes).

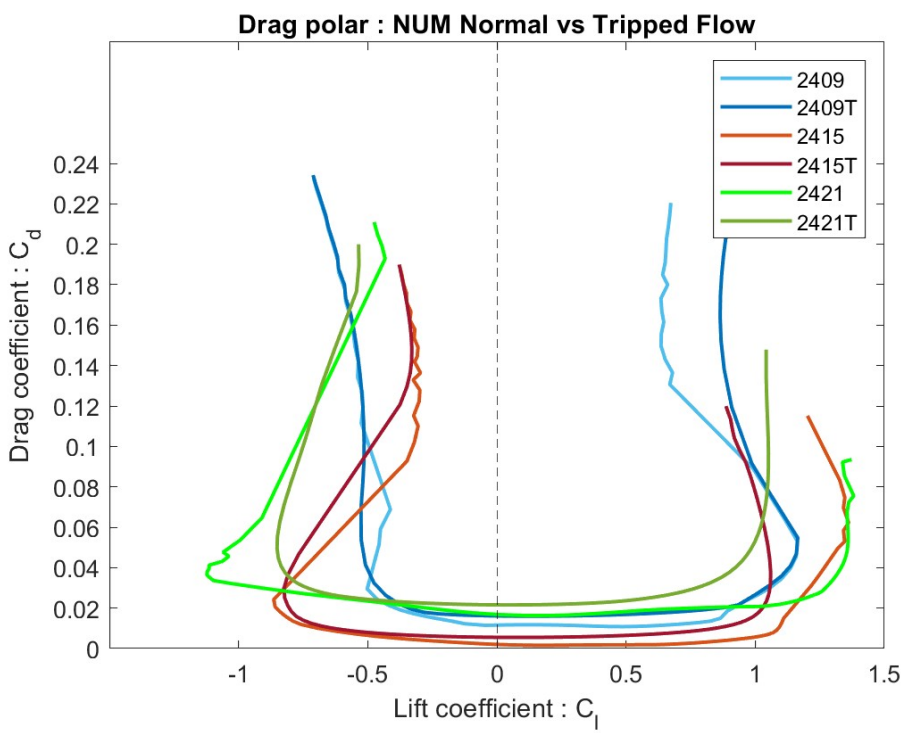
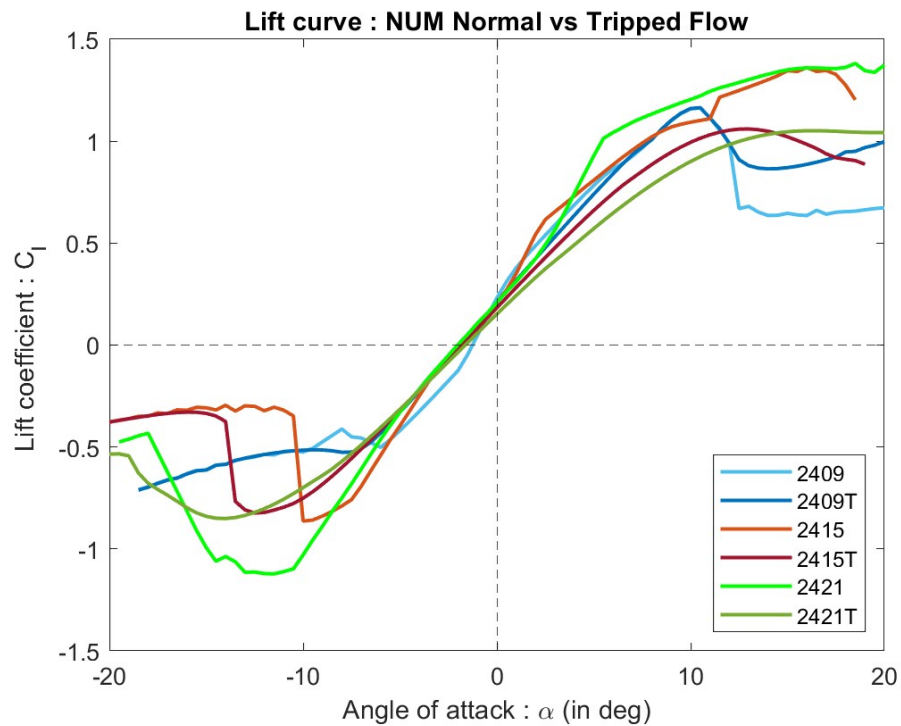
Now we shall discuss the difference between the tripped flow and the laminar flow and how the type of airflow affects our lift and drag : For this let us take as samples the NACA 2409, NACA 2415 and NACA 2421 airfoils and compare their behaviour when they are subject to tripped vs

clean airflow. This task can be done visually via the following plots:

- **Experimental Approach**



- Numerical Approach



- Analyzing the lift curves, we realize the following: the tripped flow lift curve of a respective airfoil is on average lower in the y-direction on the plot than the clean airflow case. There are many reasons this is the case, but the main reason is that the clean airflow maximizes the efficiency of the wing and extracts the most out of it, which yields a higher lift coefficient. The airfoil is much less efficient at harnessing lift when there is turbulence and both lift curve graphs back this claim.
- Analyzing the drag polars, we realize that the base of the polar curve for the clean flow (for 1 type of airfoil) is wider than the curve for the tripped flow. This is consistent for all 3 airfoil types and can be justified by the fact that again for a given drag coefficient, it is much easier to harness more lift (higher lift coefficient) in the clean airflow case as compared to the tripped one.
- The stalling occurs at the same angle of attack for both the tripped and the clean laminar airflow.
- We realize that the differences mentioned in the first and second bullets point are much more pronounced for the thicker airfoils as compared to the thinner ones. In other words, the type of flow affects much more the thicker airfoils relative to the thinner ones (the difference between the green lines is much more evident than the ones between the blue lines)

1.5 Effect of Airfoil Camber

In this section we will consider the following airfoil designs for our analysis:

NACA Number	Relative Camber
1412	-1%
2412	Reference
3412	1%

1.5.1 Results and Plots

• Analytical Approach

In order to plot the TAT lift curve we must first know the values of our zero lift angles of attack. For the **NACA 2412**, the zero lift angle of attack has been calculated :

$$\alpha_{L=0} \approx -2.1^\circ$$

For the NACA 1412 ($m = 0.01$ and $p = 0.4$) and the NACA 3412 ($m = 0.03$ and $p = 0.4$), we will use the exact same procedure as the one used for the NACA 2412 in section 1.2.1 (Therefore we will not detail the calculation in this section)

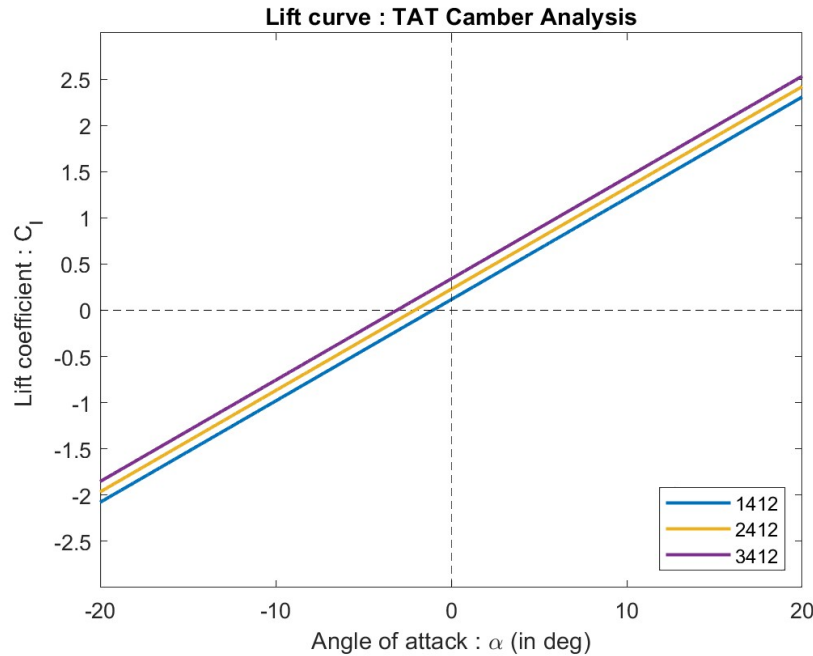
For the **NACA 3412** :

$$\alpha_{L=0} = \dots \approx -0.0182\text{rad} \approx -1.04^\circ \quad (22)$$

For the **NACA 1412** :

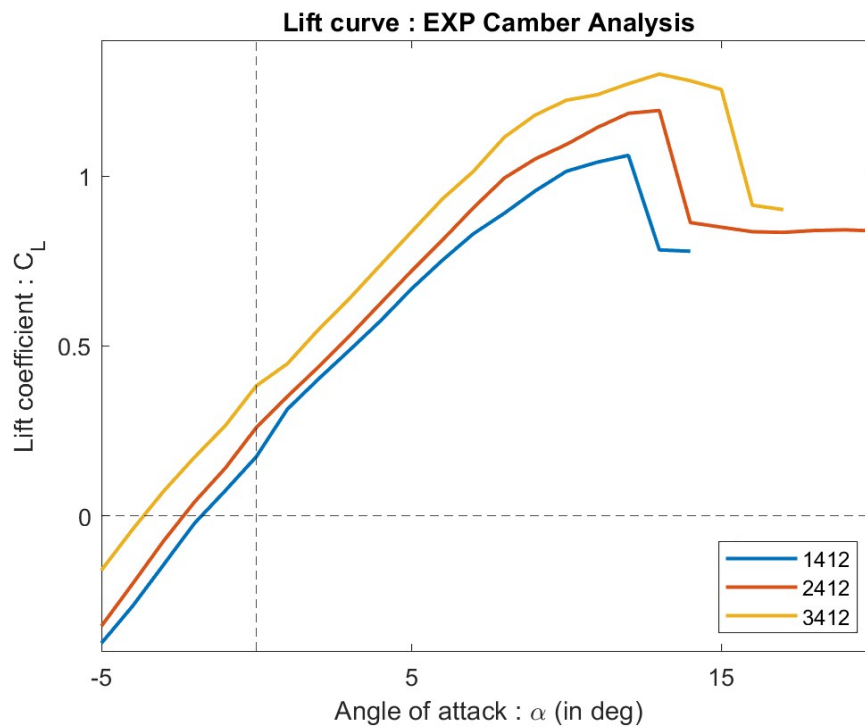
$$\alpha_{L=0} = \dots \approx -0.0544\text{rad} \approx -3.1^\circ \quad (23)$$

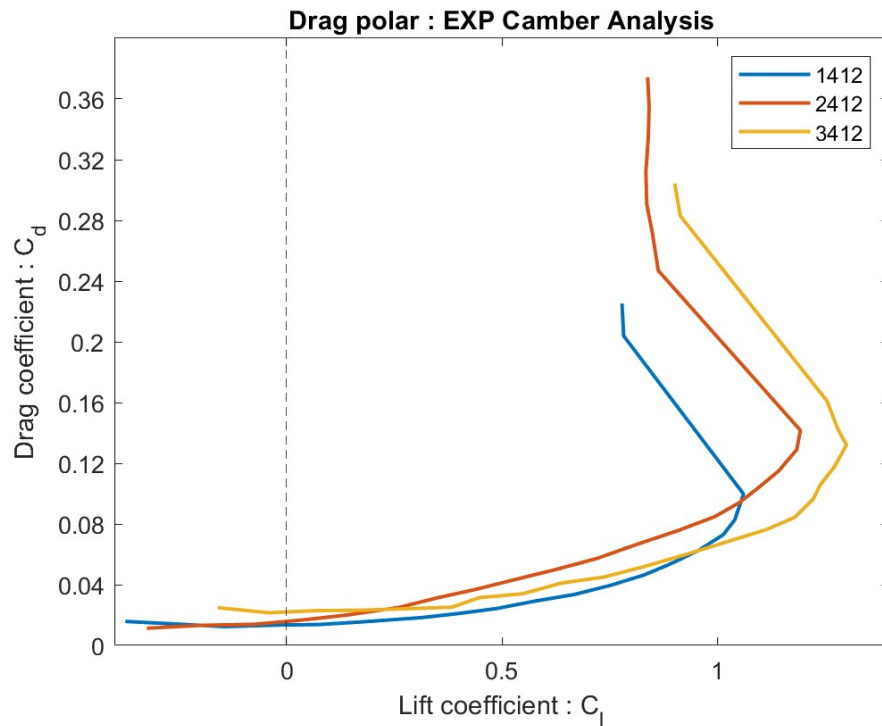
This information yields the following plot:



- **Experimental Approach**

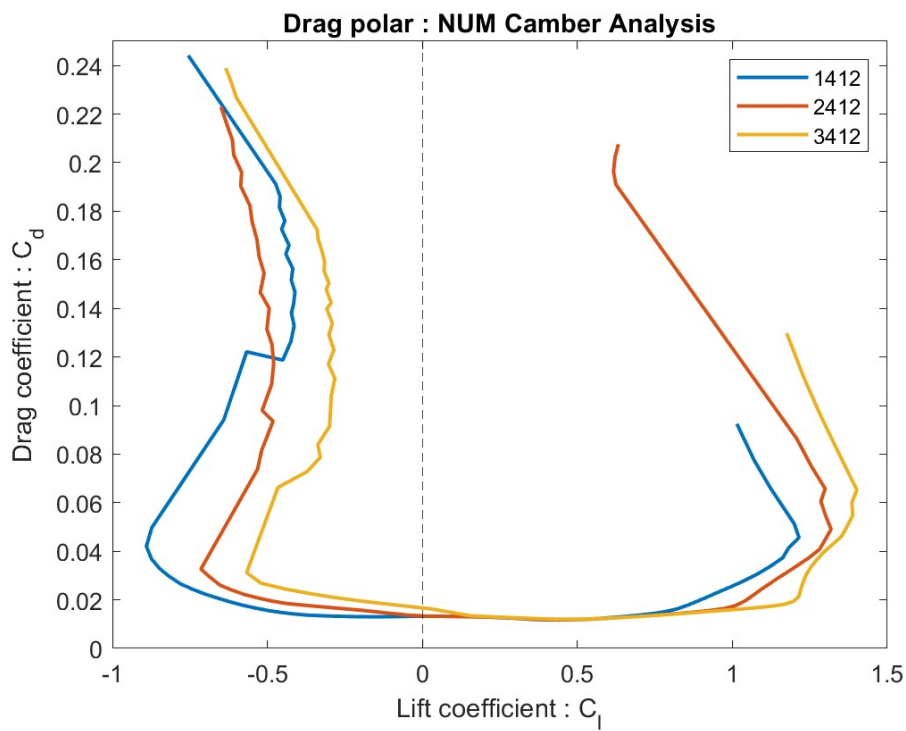
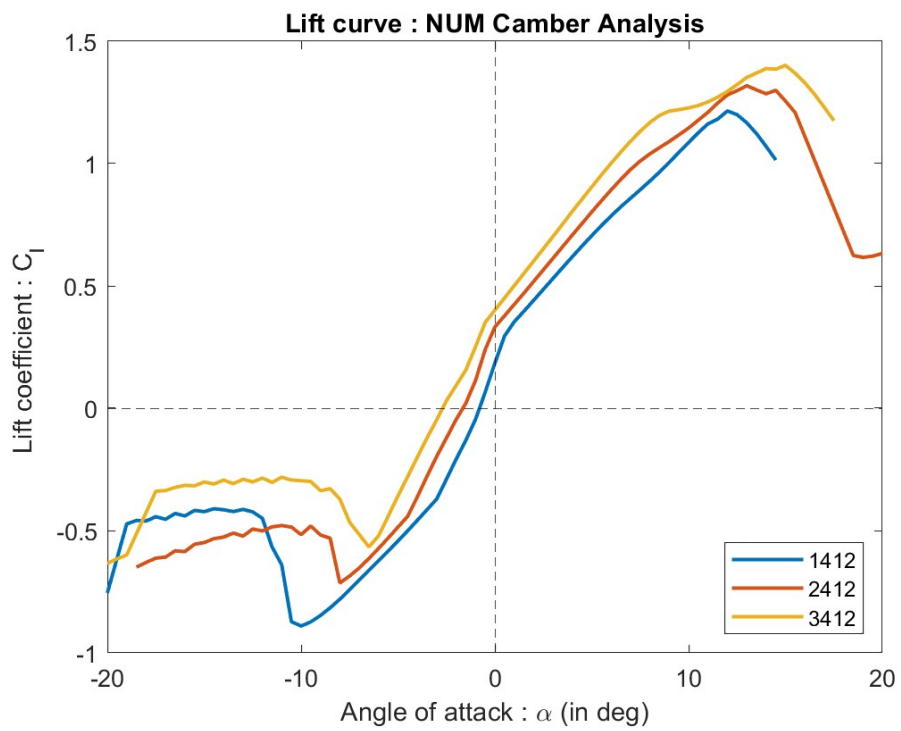
Using the same formulas as previously we can plot the following curves :





- Numerical Approach

The Numerical approach for these airfoils yields :



1.5.2 Analysis And Comparisons

Through the plots shown above we can conclude the following about the effect of airfoil camber :

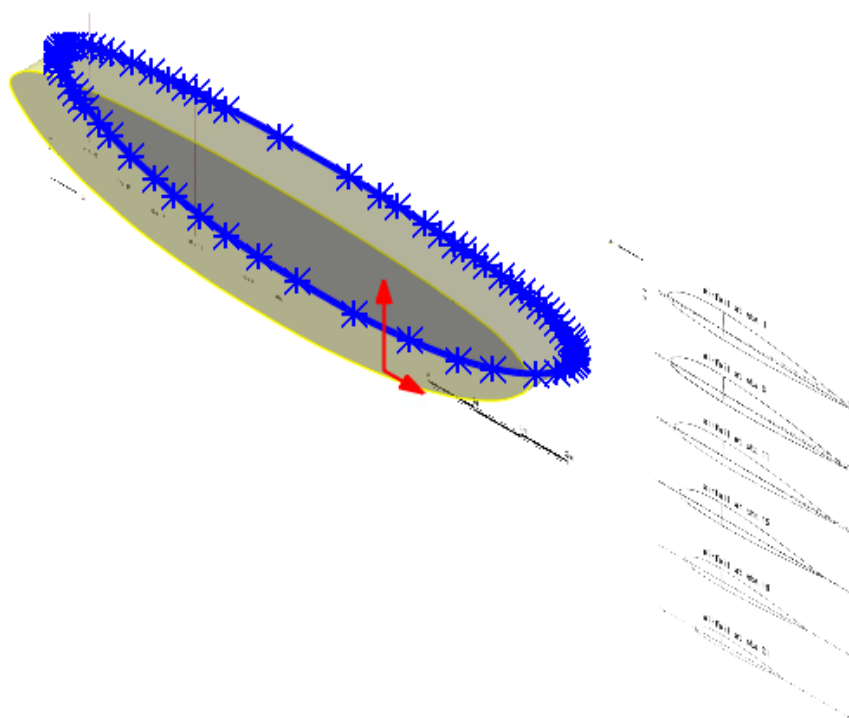
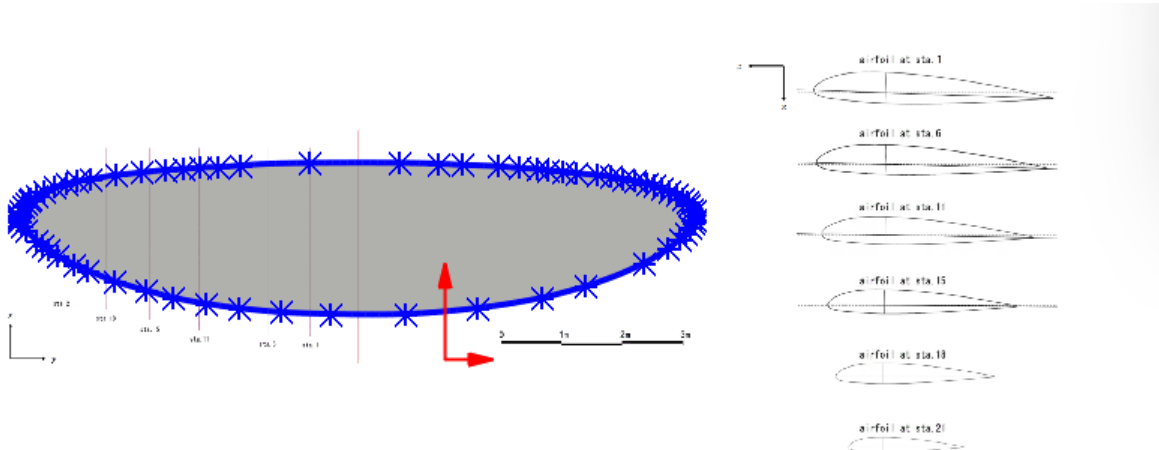
- As TAT predicts, and as is shown in the TAT plot, a higher camber has the effect of shifting the lift curve in the positive y-direction. TAT explains this by the fact that the zero lift angle of attack of a more cambered airfoil is more negative. This makes sense intuitively: At a zero angle of attack a more cambered wing will generate more lift. The data from the experimental and numerical analysis are consistent with this claim and show the vertical displacement of the lift curve.
- For positive angles of attack the stall phenomena happens later for more cambered airfoils as opposed to negative angles of attack where the stall happens at smaller angles of attack (in terms of absolute value). This means that, not only does more camber mean a shift of the lift curve in the positive y direction, but it also accompanied by a shift in the positive x direction and vice versa for less camber. As a consequence of this diagonal shift, the stall phenomena (if we consider only the stall at positive α) happens at a higher C_l for a more cambered wing.
- The "sharpness" of the stall cliff does not appear to change, meaning that the airfoil camber does not affect how brutally/smoothly the stall occurs.
- On the other hand, if we consider the drag polar curves, we note that a higher camber wing shifts the polar curves to the right. Meaning that as opposed to the thickness analysis, the drag polar curve are not symmetric with respect to a single vertical line but rather this line depends on the curve we are studying. It is important to note that for the experimental data we do not have the full data for the negative angles of attack therefore we cannot see this symmetry. Therefore, the camber artificially shifts the drag polar to the right, meaning it delays the sudden drag increase that would cause the stall. In other words, with a more cambered wing, we can achieve higher C_l without reaching the critical explosive increase in C_d which can be a very useful characteristic for an airplane especially near take-off/landing.

2 WING AERODYNAMICS

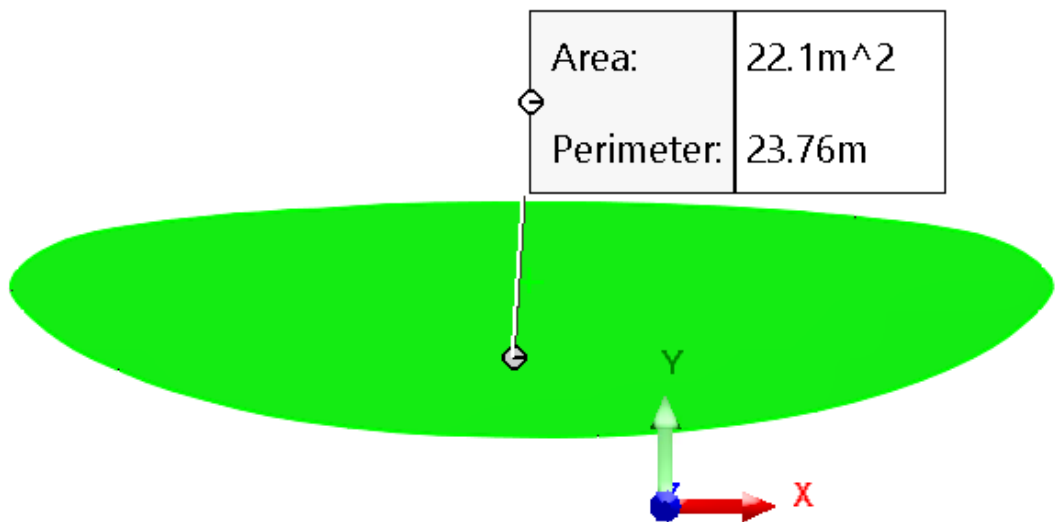
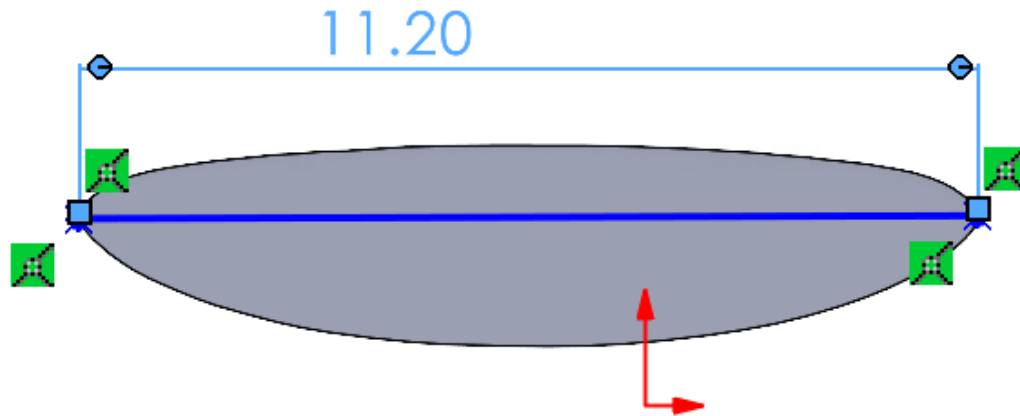
2.1 Wing Characteristics

2.1.1 Static Characteristics

In this section, we will use the information given in the PLANFORM.PNG picture to determine the geometric characteristics of the wing we will study. We are in the 21st century, therefore we will use a computer to analyze the problem. More Specifically, the wing has been modeled on SolidWorks CAD software as shown in the pictures below:



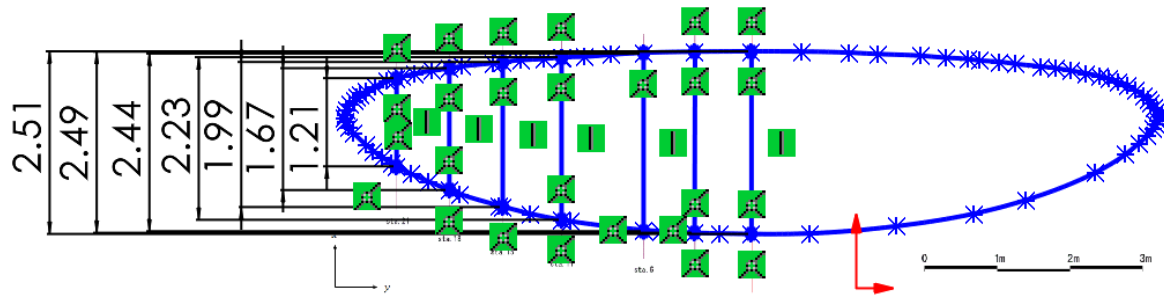
With this model we can easily conclude the wingspan and wing area :



The wingspan is deduced to be $b = 11.2m$ and the wing area is deduced to be $S = 22.1m^2$. The aspect ratio of the wing is given by :

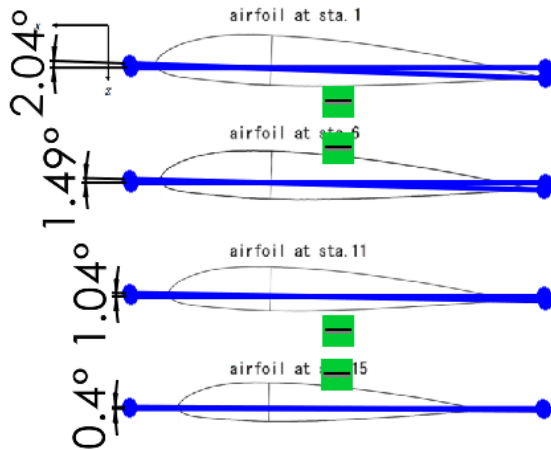
$$AR = \frac{b^2}{S} \approx 5.676$$

Now, let's observe the chord length of the wing at different wingspan locations. We have chosen 6 stations for this analysis: 1, 6, 11, 15, 18 and 21 with 1 being the wing root. The following picture and table summarizes the situation:



Station #	Chord length
1	1.21
6	1.67
11	1.99
15	2.23%
18	2.44%
21	2.49%

The angles of incidence are also deduced in a similar way :



Station #	Angle of incidence α_i (in $^\circ$)
1	2.04
6	1.49
11	1.04
15	0.4
18	0
21	0

2.1.2 Dynamic Characteristics

Now lets move on to the dynamic characteristics of the wing viz the lift coefficient C_l , the drag coefficient C_{di} and the induced angle of attack α_i . To find the values of these parameters for our wing, we must make the following assumptions:

- All assumptions imposed by LLT are supposed justifiable and respected.
- The wing is approximated as a perfectly elliptical and untwisted wing.

Our wing is designed to fly at a cruising speed of $140\text{km/h} \approx 38.89\text{m/s}$ and an altitude of $2,000\text{m}$. We are also informed that the weight of the aircraft is 5700N . At this altitude the air density is approximately 1.0066kg/m^3 . With this information and these assumptions, we can easily calculate our wing characteristics using LLT :

$$L = W = \frac{1}{2} C_l S \rho V_\infty^2 \quad (24)$$

$$\Leftrightarrow C_l = \frac{2W}{\rho S V_\infty^2} \approx 0.339 \quad (25)$$

$$C_{di} = \frac{C_l^2}{\pi A R} \approx 0.00645 \quad (26)$$

$$\alpha_i = \frac{C_l}{\pi A R} \approx 0.0190\text{rad} \approx 0.6245^\circ \quad (27)$$

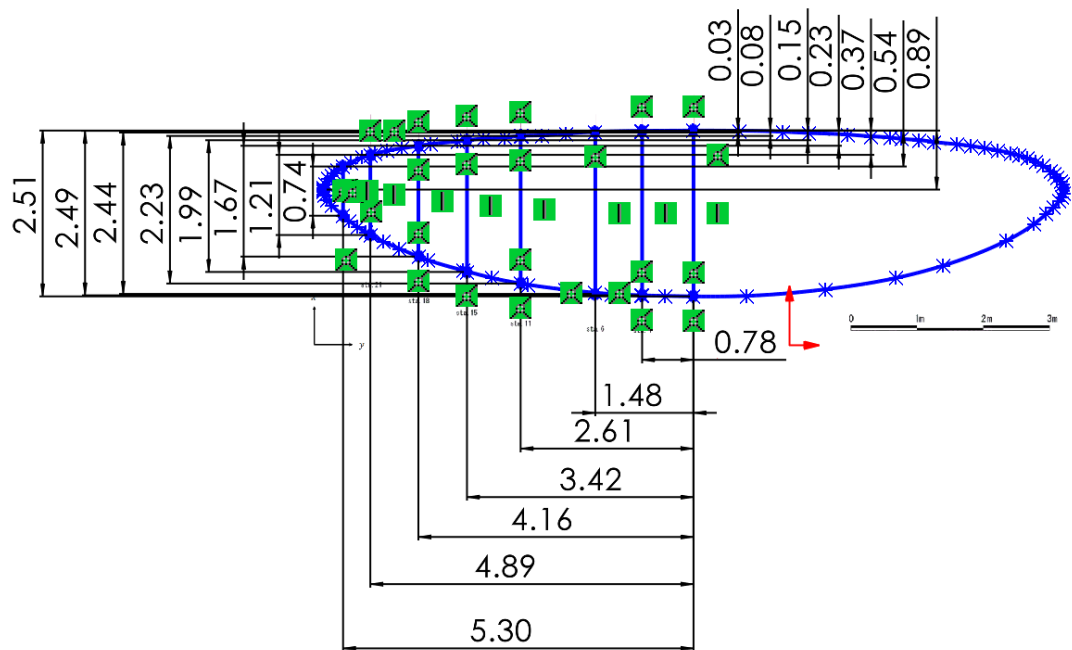
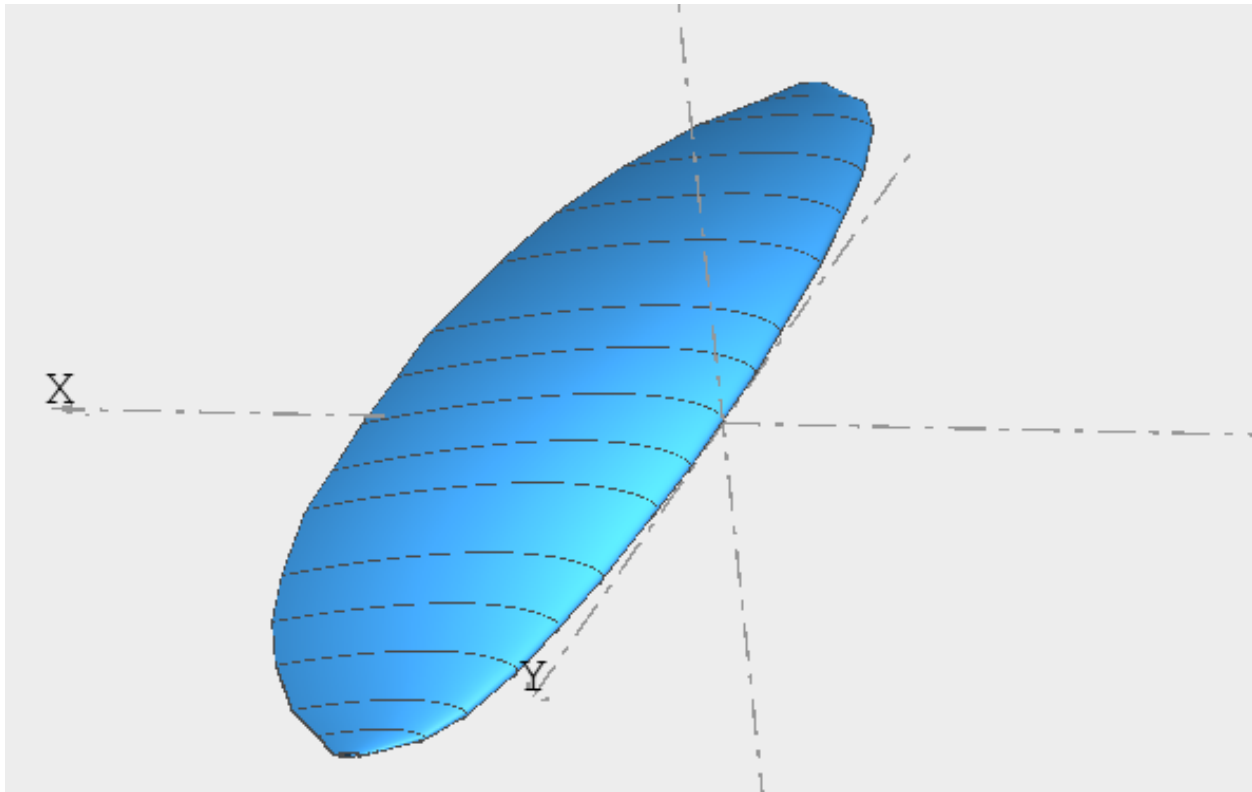
Assuming negligible viscous forces we can directly calculate our angle of attack (suppose the airfoil is NACA 2412)

$$C_l = 2\pi(\alpha - \alpha_i - \alpha_{L=0}) \quad (28)$$

$$\alpha = \frac{C_l}{2\pi} + \alpha_i + \alpha_{L=0} \approx 0.0362\text{rad} \approx 2.1^\circ \quad (29)$$

2.2 Numerical model

Using the data of our previous sections, we are able to model the geometry of our plane wing on XFLR5:



The new characteristics of the wing are as follows (due to imperfections on model):

$$S_{num} = 21.94$$

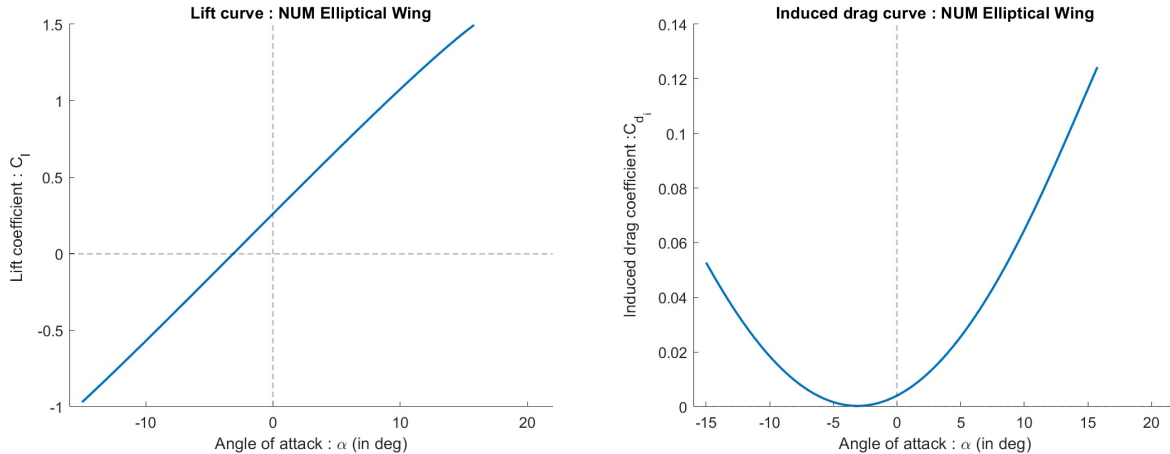
$$b_{num} = 11.2$$

$$AR_{num} = 5.72$$

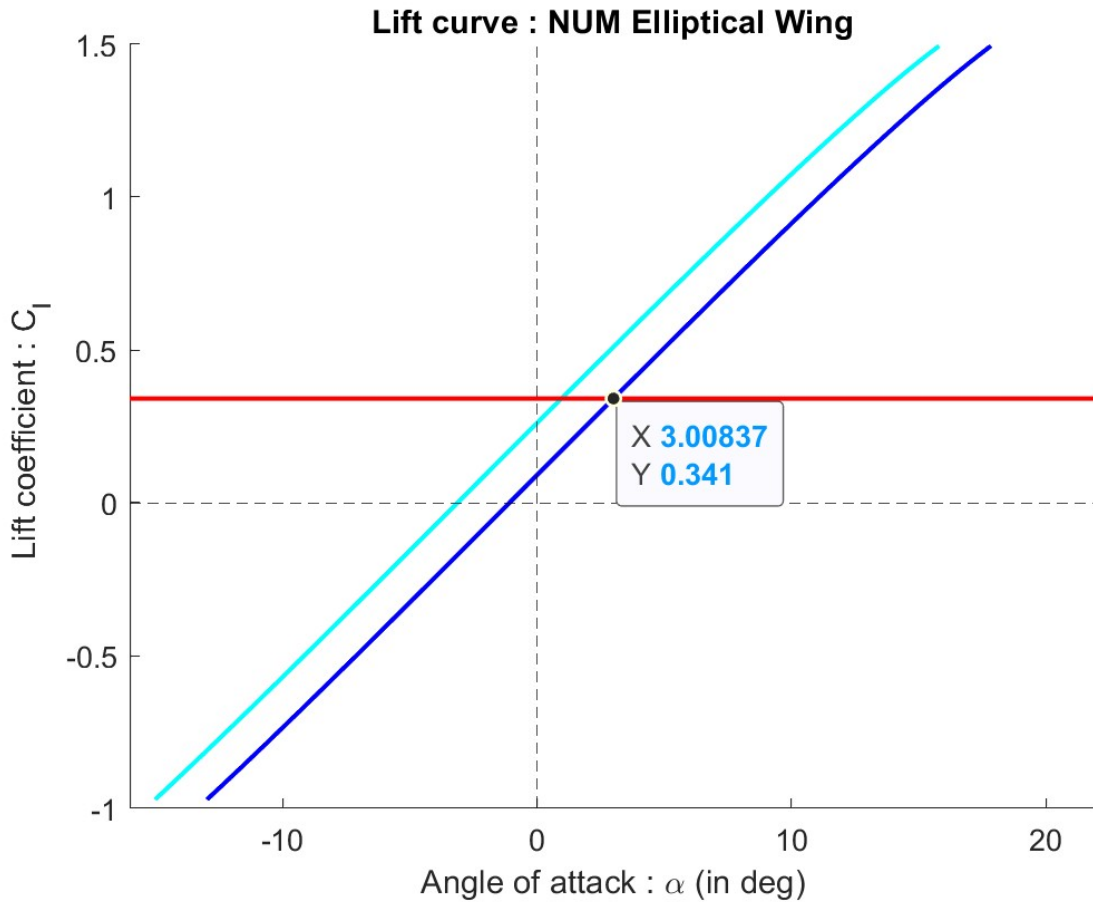
Which allows us to calculate the $C_{l_{num}}$ for the flight conditions imposed previously :

$$C_{l_{num}} = \frac{2W}{\rho S_{num} V_{\infty}^2} \approx 0.341$$

The goal now is to calculate the angle of attack predicted by the numerical method assuming the same flight conditions as previously. Firstly, it is interesting to plot the lift curve and the drag curve of our wing.:



The angle of attack predicted by the numerical simulation can easily be obtained : It is the smallest angle of attack that satisfies $C_{l_{num}} \geq 0.341$. In other words, the critical angle of attack is given by the intersection between the lift curve and the horizontal line $y = 0.357$:

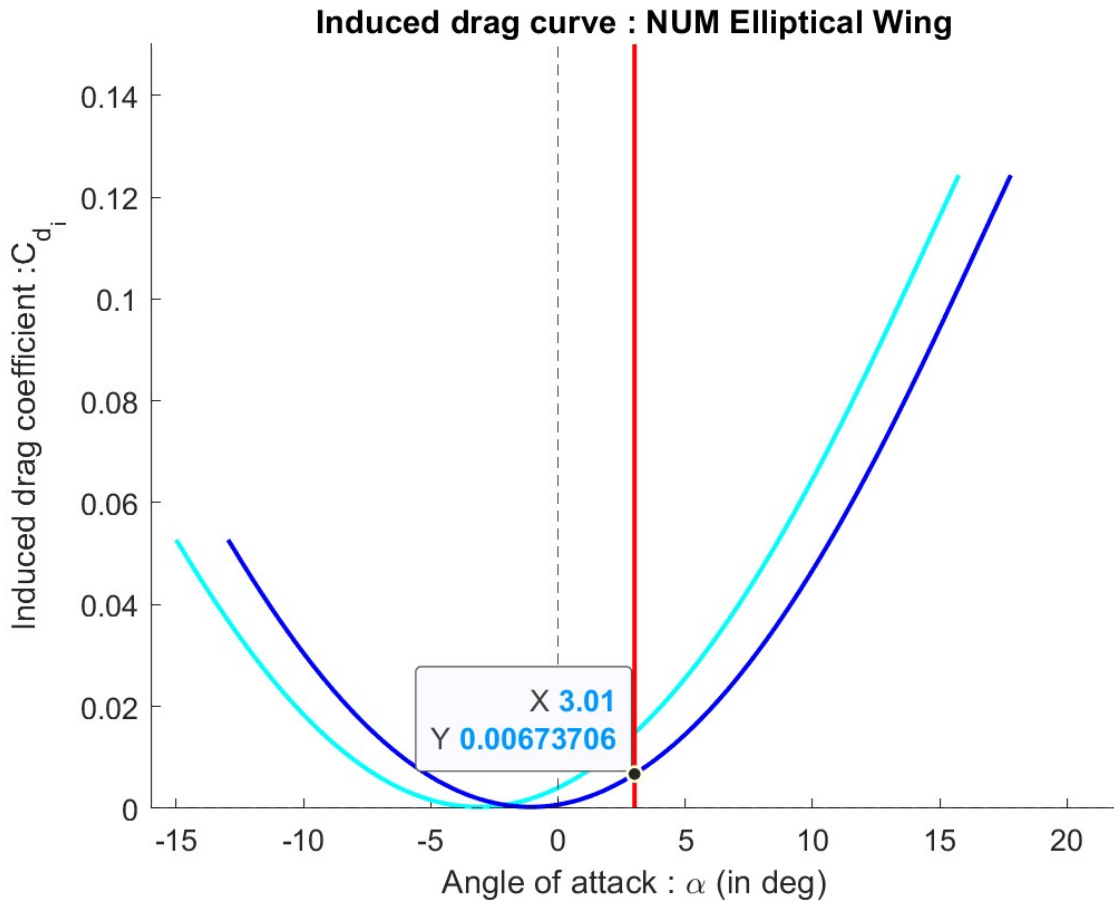


Therefore we get that:

$$\alpha_{num} \approx 3.01^\circ > \alpha \approx 2.1^\circ$$

This comparison has been discussed in the lectures and makes a lot of sense, because of viscous effects. In reality, the slope of the lift curve is slightly smaller than 2π (which we did not consider in the previous section because we supposed TAT conditions). Indeed the viscous effects will dampen the wing which is evident in this case. On another note, the fact the wing we used in the numerical test is not perfectly elliptical further justifies this comparison as a general wing has (ALWAYS) a smaller lift curve slope compared to an elliptical one. Furthermore, the effect of wing twist is to decrease the effective lift which also further explains this result.

Under these flight conditions, the induced drag coefficient can be predicted in a similar fashion. It is the intersection between the drag curve and the line $x = 3$ which represents our cruising angle of attack :



The drag induced coefficient is :

$$C_{d_{inum}} \approx 0.00674 > C_{di} \approx 0.00645$$

This again makes sense because the shape of wing used in the numerical analysis is not a perfect elliptical shape (\neq theoretical approach). The relative error can be calculated and is given by :

$$E = \frac{C_{d_{inum}} - C_{di}}{C_{di}} = 4.5\% \quad (30)$$

This means that the analysis predicts that the efficiency of an elliptical wing is around 4.5% more efficient than the planform wing we have used. However it is important to note that this difference is very small and can easily be compensated by using a security factor or a margin of error in the analytical approach.

We can also calculate the span efficiency factor (e) and the induced drag factor (δ) for both cases in order to deepen our understanding.

For the elliptical case it is very simple :

$$e = 1 \quad (31)$$

and

$$\delta = 0 \quad (32)$$

The is due to the simple geometry of elliptical wings and the fact that their shape makes it trivial to calculate it's characteristics using LLT. For the twisted uneliptical wing however we have :

$$e_{num} = \frac{C_{lnum}^2}{\pi AR_{num} C_{dignum}} \approx 0.968 \quad (33)$$

and

$$\delta_{num} = \frac{1}{e} - 1 \approx 0.0335 \quad (34)$$

It is imprtant to notice that

$$\delta_{num} \approx \delta \quad e_{num} \approx e$$

This result shows that sometimes the use of analytical tools can be very efficient, straightforward, and quick. Indeed, in this case even if our wing was a twisted non-elliptical wing, we modeled it with a perfectly elliptical non-twisted wing. And even with these assumptions, the results are relatively very, very close (even one can argue negligible). This means that we get nearly the same results without doing near as much effort. The return on the effort input is much higher in the analytical approach and that is what gives it the advantage. Also at the end of the analysis, the set of equations that explain and govern the wing characteristics are very easy to manipulate and re-use in the analytical case.

In case of doubt over misrepresenting the real result, one can use a margin of error to ensure that the results are not too far altered from the real-world scenario. Finally, it is important to note in this specific case that XFLR5 is not a very powerful tool when it comes to wing analysis.

2.3 Effect of Wing Taper Ratio

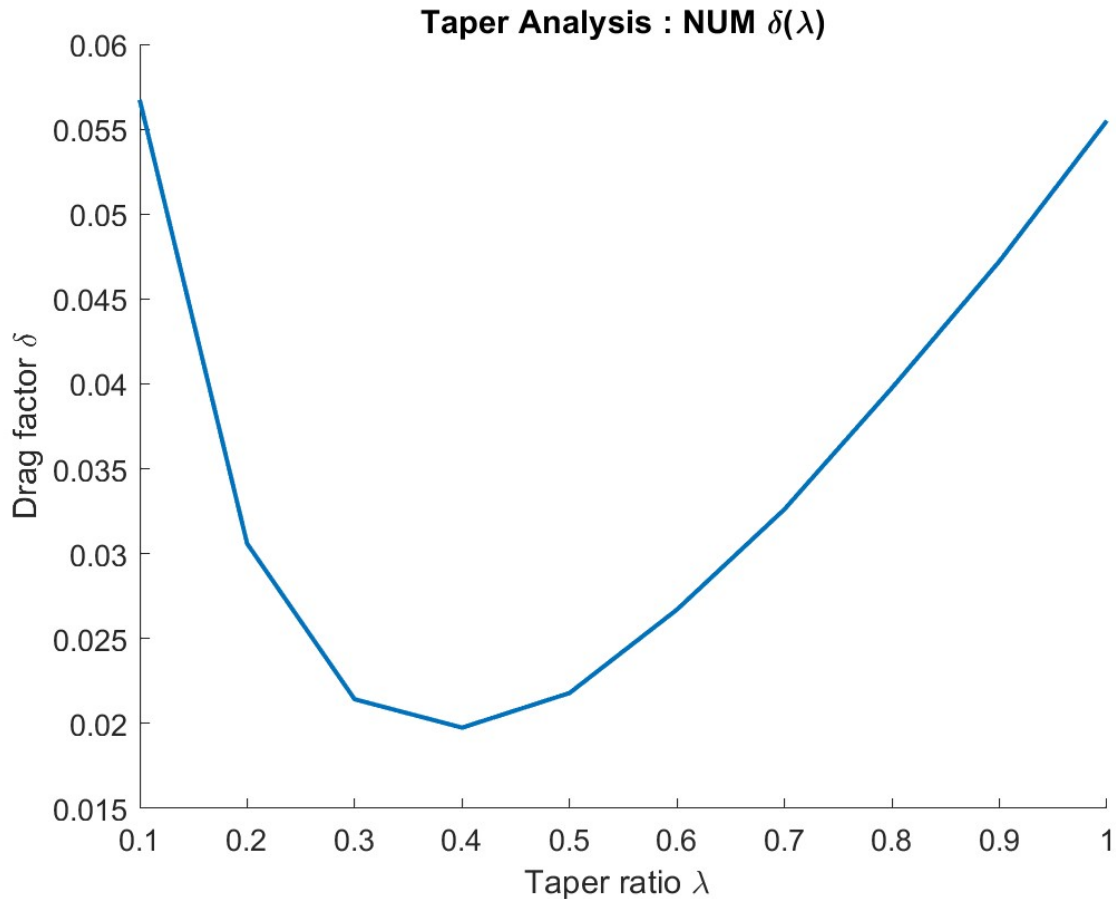
In this subsection we will consider 10 wings with 10 distinct taper ratios. It is important to note that all 10 wings share an area of $22.1m^2$, an aspect ratio of 5.676 and a NACA 2412 cross section. With these assumption we realize that the wingspan b does not change and remains constant for all 10 wings . With this information the chord length along the wing can be easily deduced :

$$S = b \frac{c_{tip} + c_{root}}{2} \Leftrightarrow b \frac{c_{root}(11 + \lambda)}{2} \Leftrightarrow c_{root} = \frac{2S}{b(1 + \lambda)} \quad (35)$$

Taper ratio (λ)	c_{root}	c_{tip}
0.1	3.588	0.359
0.2	3.289	0.658
0.3	3.036	0.911
0.4	2.819	1.128
0.5	2.631	1.315
0.6	2.467	1.480
0.7	2.321	1.625
0.8	2.192	1.754
0.9	2.077	1.869
1.0	1.973	1.973

Our goal now is to plot a curve that represents the drag factor as a function of the wing taper. We assume same flight conditions as previously and a constant angle of attack of 5° . To do this task, I have written a Matlab script. This Matlab script takes as an input the data of the 20 graphs plotted via XFLR5 for the 10 wings (2 graphs for each wing : lift curve, drag curve) and outputs 2

elements : a vector δ with the 10 drag factors of the 10 wings (from the smallest λ to the biggest). and a graph which represents this vector with respect to λ :

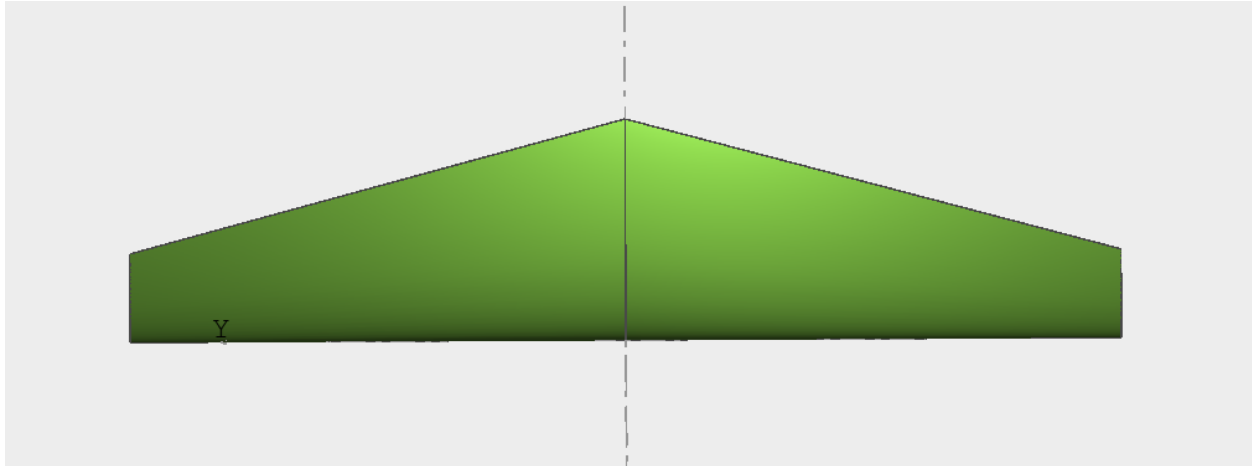


The matlab script follows these steps :

1. Opens the 20 data files:
2. For each data file it stores 2 vectors (one for α and the other either for C_{di} or C_l).
3. It finds the intersection between the line $\alpha = 5$ and C_{di} or C_l .
4. It stores the C_{di} or C_l in its respective vector (the vector that contains all drag coefficients or respectively all lift coefficients).
5. It uses equations (33) and (34) to find the value of delta.
6. It plots the desired curve .

The optimal taper ratio is obviously the one that minimizes the induced drag factor. It is easy to see and read on the previous plot that $\lambda_{optimal} = 0.4$

The shape of the wing can be seen here :



As previously discussed in the lectures, the wing shape that is most efficient in terms of induced drag is an elliptical shaped wing. And with no coincidence, it is very interesting to see that this wing looks very similar to an elliptical wing and shares it's the same overall basic shape. Although the tapered wing is a much simpler in terms of shape, the overall dimensions and geometric relations are similar. This is why today, many airplanes use a tapered wing, it offers a great alternative to elliptical wings with nearly the same efficiency but a much easier manufacturing process. On another note, Elliptical wings are very aesthetically pleasing and very cool as can be seen in the following picture of the Supermarine Spitfire (Royal Australian Airforce):



2.4 Effect of Wing Aspect ratio

2.4.1 Lift curve and Drag polar

Firstly, let us strategically choose 4 wings to analyze the effect of wing AR. For this we impose that all four wings have the same area $S = 22.1m^2$ and that they all have an optimal taper ratio $\lambda_{optimal} = 0.4$.

We choose 4 aspects ratios ranging from 2 to 8 with an increment of 2 between each one.

By defintion of the aspect ration :

$$b = \sqrt{S \cdot AR} \quad (36)$$

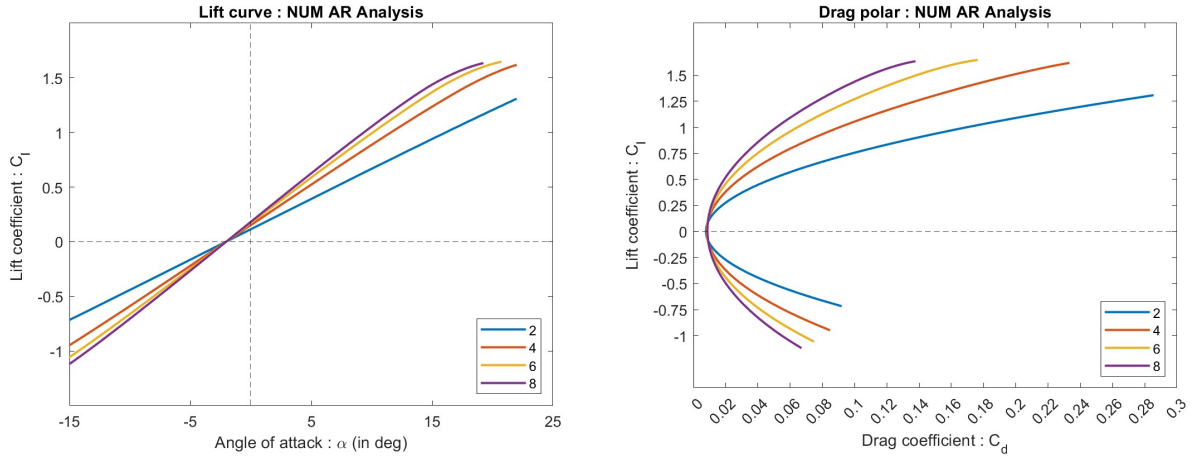
which yields

$$c_{root} = \frac{1}{1 + \lambda} \sqrt{\frac{S}{AR}} \quad (37)$$

Calculating for all our wings we get the following summary table:

Aspect Ratio AR	Wingspan b	c_{root}	c_{tip}
2	6.648	4.749	1.9
4	9.402	3.358	1.343
6	11.515	2.742	1.097
8	13.297	2.374	0.950

Let's plot the drag polar and the lift curves for our for our 4 distinctly shaped wings:



The general tendency here is actually quite prominent and pronounced:

- For the **lift curve**, the obvious tendency is that the higher the AR of the wing, the steeper the slope of the curve is. This is especially obvious for the wing with AR = 2 that has a much shallower slope than the others. The difference in slope is explained by the induced drag being smaller for high AR wings (due to a smaller wingtip vortex). It is important to note that the zero lift angle of attack is the same for all wings despite the fact that they don't share the same geometry (The airfoil remains a NACA 2412).
- For the **drag polar**, it is also easy to notice the overall width of the curve increases as a function of the AR. In other words, for a given C_d the distance separating the 2 lift coefficients (that satisfy this C_d) of a given curve increase with respect to the AR. Physically what this means is that if we specify a certain C_d , the wing with the higher AR will be able to generate

more lift compared to the one with lower AR.

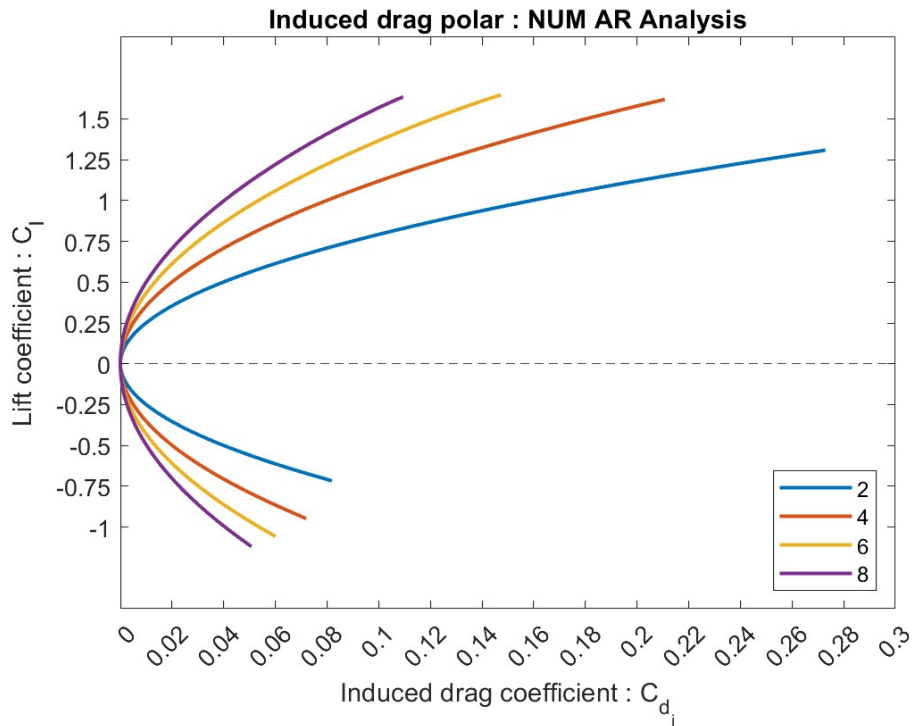
Now, note that the tail ends of the curves are further shifted to right for the lower AR wings. This also means that the lower AR wing will stall at a later point compared to the higher AR wings.

So to conclude: The higher AR wings are able to generate more lift at the cost of stalling earlier and more suddenly.

When designing an aircraft, it is important to maximize the lift that the wing can potentially generate but also to avoid stall. More specifically to avoid stall at a small angle of attack but also to avoid sudden sharp stall. Therefore, it is important to take into account all the specific requirements and constraints of the aircraft's mission and to use this valuable information to choose a balanced AR wing that generates enough lift whilst maintaining a safe and stall-free environment. Also, both extremes (high AR and low AR) should be avoided at all costs(except for very extreme circumstances)

2.4.2 Induced drag Analysis

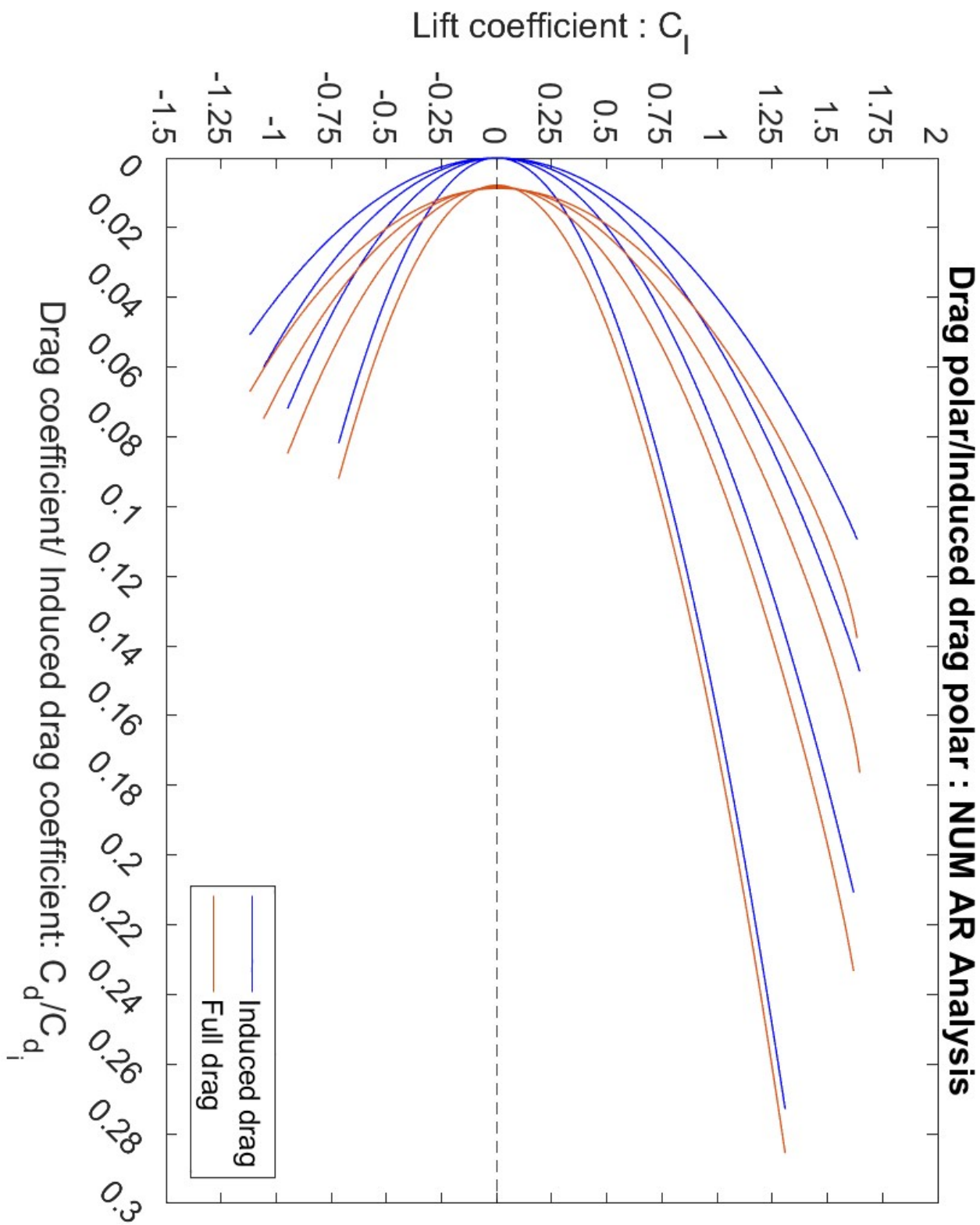
It is important to note that the drag polar takes into account all drag. Another interesting polar to draw is the induced drag polar that only takes into account the induced drag:



We can immediately see similarity in shape and behavior between this drag polar and the previous one. To further enhance our comparison lets draw both polars on the same plot:

A couple of remarks here:

- In general, the IDP is a shifted (to the left) version of the original DP. This is very logical, as the full drag is the sum of the induced drag and the viscous drag. Therefore it would not make sense if the IDP was shifted to the right compared to the DP (That would mean that

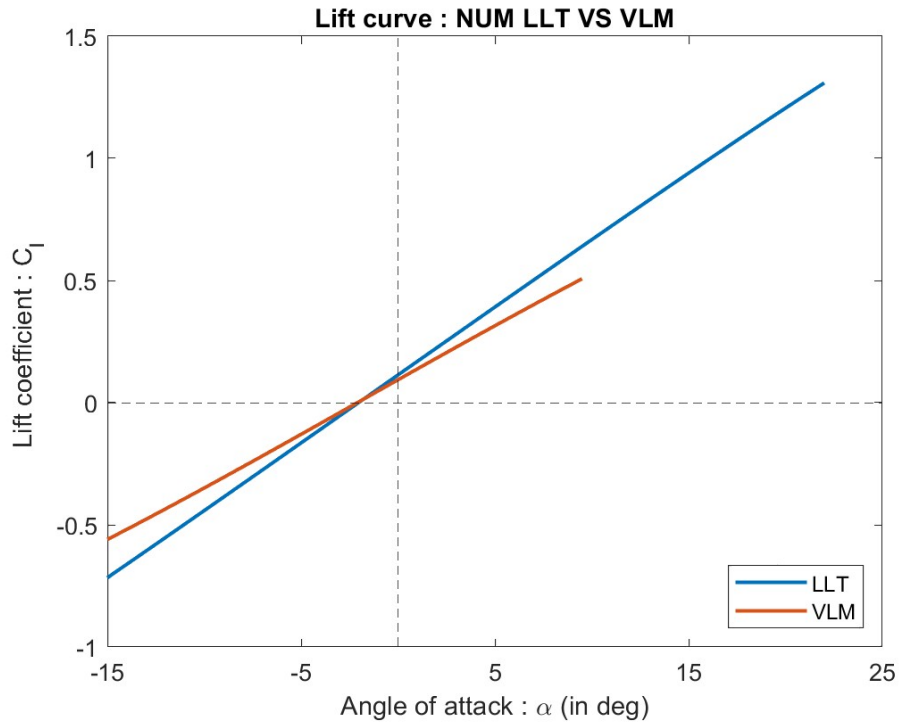


the laws of physics are broken). This shift to the left, imposes that, as the theory suggests, the induced drag is always smaller than the full drag.

- It is important to note that the induced drag is 0 for a $C_l = 0$ as opposed the full drag (due to the viscous forces). Indeed the induced drag is directly proportional to the square of the lift coefficient (which explains the parabolic shape).
- Finally we notice that the difference between the IDP and the DP is always bigger for the higher AR Wings. This, in my opinion, is a consequence of the fact that the boundary layer is amplified and accumulates much more for the higher AR (due to the overall higher chord lengths of the wings). Also as we mention in the next section, LLT is potentially not very accurate for low AR wings.

2.4.3 VLM VS LLT

The following plot shows the lift curve of the $AR = 2$ wing used in the previous section. We have used 2 numerical models to draw this lift curve : Classic LLT and VLM



The plot highlights a key difference : VLM predicts a smaller slope for the lift curve compared to LLT. This means that VLM predicts an even worse efficiency of this already very inefficient wing. The zero angle of attack is unsurprisingly the same for both models.

It is important to emphasize that we are studying an $AR = 2$ wing which is very weird and non-conventional shaped wing with a huge root chord length.

VLM uses in the background surface panels and vortexes on them to model the situation (as opposed to lines in LLT). The fact that VLM is based on surfaces makes it much more attractive candidate and will probably enable it to predict more accurately the situation. The LLT conditions don't match this specific problem because the wing cannot easily be replaced by a vortex line and needs a more complex surface due to its weird shape.

2.5 Conclusion and final results

In this final section, we shall combine all the information concerning the lift curves in all the previous sections and compare all the results. We have chosen the following data to analyze and have plotted everything in a single curve:

1. The airfoil using TAT
2. The airfoil using experimental measurements in a wind tunnel
3. The wing (untwisted) using the numerical LLT scheme in XFLR5.
4. The wing (twisted) using the numerical LLT scheme in XFLR5
5. The optimally tapered wing (untwisted) using the numerical LLT scheme in XFLR5
6. The rectangular wing (untwisted) using the numerical LLT scheme in XFLR5
7. The optimally tapered wing (untwisted) with $AR = 4$ using the numerical LLT scheme in XFLR5.
8. The optimally tapered wing (untwisted) with $AR = 8$ using the numerical LLT scheme in XFLR5.

A couple of interesting remarks to analyze here :

- The TAT lift curve stands our from the pack. This is (again) due to the assumptions of TAT that neglect viscosity and suppose a potential flow which leads to lift curve slope that is bigger than the other candidates. (viscosity tends to lower the slope).
- The experimental curve also stands out due to the early stall cliff. This shows that the numerical data is not necessarily perfect, specially with 3D wing modeling on XFLR5. Also the experimental data is the only one that is a bit similar to the TAT data. This is due to the fact that the experiment was testing for the airfoil, and was setup in a way to avoid 3D effects such as wingtip vortices (Vortex= Induced drag = Smaller slope).
- The untwisted wing seems to perform better than the twisted wing. This comes as no surprise. The point of twisting a wing is simply to stabilize the plane. But in physics, everything comes at a price and the price paid here to stabilize the plane is higher drag and lower lift(which is shown on the plot)
- The zero lift angle of attack, or more visually the intersection between the lift curves and the x-axis are all nearly the exact same for all the data. This comes as no surprise as the airfoil used is a NACA 2412 in all cases and the camber does not change. There is however, one exception to this and that is the twisted wing. This again is expected from the twisted wing and comes from the fact that the angle of attack at certain point in time is different depending on the position along the wing. The fact the angle at the tip is lower then at root (washout) causes an overall "average" of angles along the wing that is lower then the value of the angle at the root which This why the zero lift angle of attack is smaller for the twisted wing compared to other wings.
- Finally, the tapered wing performs (as expected) slightly better than the rectangular wing (the tapered lift curve is slightly above the rectangular lift curve). This is consistent with the fact that the tapered wing is the more efficient than the rectangular one (and is a simpler iteration of the elliptical wing).

